Earth-Science Reviews 189 (2019) 220–243

Contents lists available at ScienceDirect

Earth-Science Reviews

journal homepage: www.elsevier.com/locate/earscirev

A multidisciplinary approach to review the vertical and lateral facies relationships of the purported vertebrate-defined terrestrial Permian–Triassic boundary interval at Bethulie, Karoo Basin, South Africa

Robert A. Gastaldo[a,*], Johann Neveling[b], John W. Geissman[c], Jiawen Li[a]

[a] Department of Geology, Colby College, Waterville, ME 04901, USA
[b] Council for Geoscience, Private Bag x112, Silverton, Pretoria 0001, South Africa
[c] Department of Geosciences, The University of Texas at Dallas, Richardson, TX 75080-3021, USA

ARTICLE INFO

Keywords:
Permian–Triassic boundary
Mass extinction
Rock magnetism
Dicynodon
Lystrosaurus

ABSTRACT

The stratigraphic section at Bethulie, South Africa, is reported to contain the vertebrate-defined Permian–Triassic boundary succession in the terrestrial realm of the Karoo Basin. The model of vertebrate turnover, from the *Daptocephalus* to *Lystrosaurus* Assemblage Zones, tightly constrains the boundary sequence to a short stratigraphic interval where siltstone color begins to change from greenish gray to grayish red, the latter color interpreted to be a consequence of aridification. The biological response to this facies change has been termed "the Great Dying," and the sedimentary rocks that are preserved are ascribed to a playa lake depositional setting. This drying event is believed to be contemporaneous across the basin, although previous studies have shown that the facies appears at multiple horizons at all purported Permian–Triassic boundary sections in the basin.

Here, we report results of a multidisciplinary effort to characterize the vertebrate assemblage-zone boundary interval exposed at Bethulie using the lithostratigraphic, petrographic, geochemical, and rock magnetic properties of these rocks. In this stratigraphic succession at its "type" location, the 3-m thick assemblage-zone boundary interval is distinguished by thick beds of greenish-gray, greenish-gray mottled to grayish-red, and grayish-red siltstone, all of which change facies characteristics laterally along strike. Specifically, about 220 m to the southeast of the type section, sediments lose all grayish-red coloration, whereas the interval becomes laminated to the northwest. Petrographically, most siltstone is homogenized, with few burrows and small-scale cross-bedded structures with mudchips. There are no gypsiferous or calcareous beds, nor is there evidence of disturbed structures, authigenic breccia, or pseudomorphs associated with dessication. Mean elemental composition of both greenish-gray and grayish-red beds are indistinguishable, geochemically, and both are dominated by illite and chlorite clay species. Mössbauer spectroscopic analyses reveal the presence of a small concentration of fine-grained hematite in the grayish-red siltstone, with its presence mainly found as coatings on clay minerals. Rock magnetic experiments (isothermal remanent magnetization, acquisition and backfield DC demagnetization; magnetic hysteresis; susceptibility vs. temperature) yield data that demonstrate no essential differences between the different colored siltstones. And, both lithologies host mangnetite/maghematite and hematite. Our results do not support the previous interpretation that this inferred Permian–Triassic boundary interval represents the onset of playa lake deposits under conditions of aridification. Rather, our evidence supports the existence of a "wet" landscape at what is considered the *Daptocephalus/Lystrosaurus* assemblage-zone boundary.

1. Introduction

The vertebrate biostratigraphic record in the Beaufort Group of the Karoo Basin, South Africa, is widely accepted as preserving the terrestrial response to the end-Permian extinction event (Ward et al., 2005; Smith and Botha-Brink, 2014; Rubidge et al., 2016). Megafaunal vertebrate turnover, which has been associated with events in the marine record by several workers (Shen et al., 2011; Benton and Newell, 2014; but see Gastaldo et al., 2015, Neveling et al., 2016a, 2016b), focuses on the transition from the *Daptocephalus* (formerly *Dicynodon*; Viglietti

* Corresponding author.
E-mail address: ragastal@colby.edu (R.A. Gastaldo).

http://dx.doi.org/10.1016/j.earscirev.2017.08.002
Received 30 April 2017; Received in revised form 28 July 2017; Accepted 3 August 2017
Available online 08 August 2017
0012-8252/

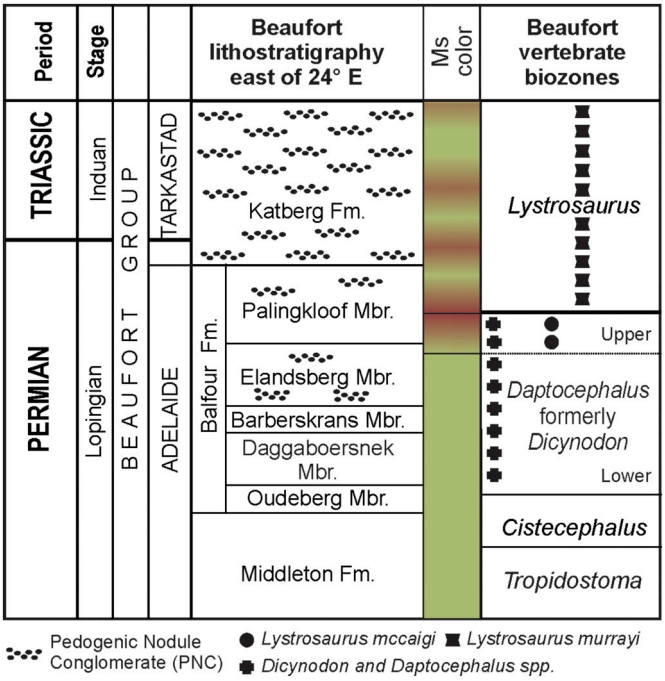

Fig. 1. Generalized stratigraphy of the Karoo Supergroup spanning the upper Carboniferous into the lower Triassic, following Johnson et al. (2006). Vertebrate assemblage zones after Viglietti et al. (2016). Previous workers have placed the Permian–Triassic Boundary (thick solid line) at the contact between the *Daptocephalus* (formerly *Dicynodon*) and overlying *Lystrosaurus* Assemblage Zone (Ward et al., 2005; Smith and Botha-Brink, 2014; Rubidge et al., 2016). Placement of the PTB in the Tarkastad Subgroup follows the recommendation of Gastaldo et al. (2015), based on an early Changshingian maximum age date in the upper *Daptocephalus* AZ, that the boundary, if represented in the sedimentary record, occurs in the Katberg Formation.

et al., 2016) to the *Lystrosaurus* Assemblage Zone (AZ; Fig. 1). Recently, though, Lucas (2017a, 2017b) argues that the proportion of systematic turnover across the biozone boundary is not significantly higher than background extinction rates. And Lucas (2017a, 2017b) concludes that late Permian tetrapod extinctions in the Karoo Basin appear to be older than the crisis in the end-Permian marine record and, hence, are not coincident. Nevertheless, other workers continue to apply a long-held paradigm that is based on the assumptions of early workers when the relative age of the Beaufort Group rocks were yet constrained by geochronometric means.

Broom (1906) was the first to assign a Triassic age to the *Lystrosaurus* Zone with all underlying vertebrate zones, including the *Daptocephalus* AZ (see Lucas, 2017b who argues for a return to the use of the *Dicynodon* AZ) to the late Permian. No empirical basis for the age assignment of any vertebrate biozone is provided in the literature, and these may be a consequence of prevailing assumptions at the time. Unchallenged for more than a century, the Permian age for the *Daptocephalus* and underlying vertebrate assemblage zones seemingly was based on a more robust biostratigraphic correlation of the *Cistecephalus* AZ (Smith and Keyser, 1995) with better dated Indian (Kutty, 1972), South American (Keyser, 1981), and Russian (Boonstra, 1969) successions. Confirmation of a Permian age assignment for the *Cistecephalus* and underlying assemblage zones only occurred in the past few years with the publication of U-Pb ID-TIMS age estimates for the Adelaide Subgroup by Rubidge et al. (2013; Fig. 1). Yet, no marker horizons in the uppermost two vertebrate biozones of the Beaufort Group–-*Daptocephalus* and *Lystrosaurus* AZs–that could be dated by geochronometric methods have been reported until recently (Gastaldo et al., 2015). Prior to that report, paleontological correlation was the basis for a relative Triassic-age assignment of the *Lystrosaurus* AZ due to its close association with the overlying *Cygnognathus* AZ of known Triassic age. As a consequence, an Early Triassic age for the *Lystrosaurus* AZ and a latest Permian age for the *Daptocephalus* AZ was widely accepted when research began to focus on the response of the terrestrial ecosystem to the end-Permian crisis near the turn of the last century when a model emerged.

1.1. Origin of an extinction model

Smith (1995) first described a Permian–Triassic boundary section from what has been referred to in the literature as the Bethulie locality in the Free State Province. At that point in time, the stratigraphic ranges of the *Daptocephalus* (*Dicynodon*) and *Lystrosaurus* AZ faunas were thought to be non-concurrent (Keyser, 1981; Keyser and Smith, 1978), even though Hotton (1967) reported overlap in the stratigraphic ranges of the index taxa. This latter observation was confirmed by the biostratigraphic ranges presented by Smith (1995, his Fig. 3). He showed a sharp turnover at the contact between the *Daptocephalus* and *Lystrosaurus* AZs, with the First Appearance Datum (FAD) of *Lystrosaurus* 25 m beneath the biozone boundary. While acknowledging that the Permian–Triassic boundary (PTB) is not clearly defined, Smith (1995) interpreted the apparently sharp turnover to represent the end-Permian extinction event in order to maintain uniformity with the more severe extinction recorded in the marine realm. Thus, the boundary was correlated with "…the uppermost occurrence of the *Dicynodon* (*Daptocephalus*) Assemblage Zone fauna…" (Smith, 1995, p. 86), placed near the base of the Palingkloof Member. This assignment, though, contradicts later claims (Smith and Ward, 2001; Ward et al., 2005) that the base of the *Lystrosaurus* AZs was traditionally associated with the base of the Katberg Formation.

Rocks in which the *Daptocephalus* AZ fauna is preserved are reported to be dominated (~80%) by grayish (blueish gray, dark gray, greenish gray) and even some purple siltstones, in which fine-grained single story (4–8 m thick) and multistory (10–25 m thick) ribbon sandstones and thin sheets are enveloped. Most workers agree with Smith's interpretation that these sediments accumulated in a meandering fluvial setting. It should be pointed out, though, the meanderbelt exposures on which Smith (1995, p. 87, his Fig. 5) has based this interpretation are exposed at the Reiersvlei locality, which occurs at a lower stratigraphic position in the Beaufort Formation and geographically is situated > 400 km to the southwest (Smith, 1987) of Bethulie. A color change to reddish brown characterizes the siltstones of the Palingkloof Member (reportedly > 40 m thick) at Bethulie, combined with an increase in the frequency and thickness of sheet sandstones. These sandstone bodies are < 5-m thick and reported to contain upper flow-regime sedimentary structures that include gullied bases draped by matrix-supported intraformational conglomerate. This conglomerate consists of siltstone and pedogenic nodular (glaebules) clasts. The latter also may occur as isolated lenses in the siltstone. This interval was interpreted as having been deposited in wide, shallow, ephemeral streams that were the precursors of the braidplains associated with Katberg deposition (Smith, 1995).

Pedogenic features associated with the greenish-gray siltstone of the *Daptocephalus* AZ from this interval were interpreted to reflect soil formation under a warm climate and strong seasonality with an overall a high water table. In contrast, the reddened, calcic soil horizons of the overlying *Lystrosaurus* AZ, together with an increased frequency of articulated vertebrate remains, were believed to be associated with warm, semi-arid climatic conditions. Following Hiller and Stavrakis (1984), Smith (1995) envisaged both tectonic and climatic factors to have been responsible for the changes in the fluvial style across this interval, considering the tectonic processes to have been the primary driver. A change from a high- to low-sinuosity fluvial environment was attributed to a pulse of tectonism in the Cape Fold Belt. Associated with this tectonic pulse was the initiation of regional aridification over southern Gondwana that also was linked to a decline in tetrapod diversity during the latest Permian. In this initial model, the tectonically induced change in fluvial regime introduced basinward migration of dry floodplain

environments, which allowed the dry-adapted *Lystrosaurus* communities to colonise the central parts of the basin to the detriment of the *Daptocephalus* fauna that lived there. These communities were considered to have co-existed for a short period until a combination of shrinking habitat and competition resulted in the disappearance of the *Daptocephalus* AZ fauna.

1.2. Refinement of the extinction model

1.2.1. Stratigraphy

Using the previous work of Smith (1995), Ward et al. (2000) introduced a sedimentological model for the PTB interval wherein these authors circumscribed three distinct lithofacies associations associated with the pre-, boundary event, and post-extinction landscape. Subsequently, the model evolved to encompass five distinct lithofacies associations primarily based on two sections near Bethulie (Free State Province) and five sections near Lootsberg Pass (Eastern Cape Province; Ward et al., 2000; Smith and Ward, 2001). Later, these localities were augmented by data reported from Carlton Heights (Retallack et al., 2003; Ward et al., 2005), Commandodrif (De Kock and Kirschvink, 2004; Ward et al., 2005), and Ripplemead (Smith and Botha-Brink, 2014). A new boundary locality was described from the farm Nooitgedacht 68 in Free State Province (Botha-Brink et al., 2014). The boundary sequence, from bottom to top, can be summarized as follows.

1.2.1.1. Lithofacies association A. The base of the succession is characterized by massive, greenish-gray siltstone that predominates with subordinate, thick, single storied sandstone bodies (Ward et al., 2000)., This interval has been interpreted to represent meandering fluvial deposits (Smith and Ward, 2001; Smith and Botha-Brink, 2014) based on the presence of low-angle (10–15°) lateral accretion surfaces that typically extend throughout the thickness of the channel sandstone and into the overlying siltstone deposits (Ward et al., 2000). Lithofacies association A is thick, reported by Smith and Botha-Brink (2014; their Fig. 3) to be > 40 m at Bethulie in the Elandsberg Member. The largest diversity of vertebrate fossils belonging to the *Daptocephalus* AZ are reported from this interval (Smith and Ward, 2001).

1.2.1.2. Lithofacies association B. The overlying lithofacies consists of an interval of massive, mottled maroon and greenish-gray mudrock, with thin tabular sandstone bodies that display distinctive “gullied” basal contacts (Smith and Ward, 2001; Smith and Botha-Brink, 2014). In past model versions, lithofacies association B was part of the Lithofacies Association A (Ward et al., 2005; Smith and Botha, 2005; Botha and Smith, 2006). Smith and Botha-Brink (2014; their Fig. 3) restrict this lithofacies association to only an approximately 15-m thick succession at Bethulie which also is placed in the Elandsberg Member and the lowest few meters of the Palingkloof Member. Smith and Ward (2001) reported a single horizon of “large brown-weathering calcareous nodules” from the uppermost siltstone of this interval, which they considered the lithological expression of the PTB. Subsequently, the uppermost concretion-bearing siltstone was referred to as the End-Permian Paleosol at Carlton Heights (EPP; De Kock and Kirschvink, 2004), but the concept appears to have been abandoned in nearly all subsequent papers (see Coney et al., 2007 who continued to use this concept). Fossil remains of the *Daptocephalus* AZ are comparatively rare in this second unit (Smith and Botha, 2005), while the ichnogenus *Katbergia* (Gastaldo and Rolerson, 2008) reportedly makes its first appearance in this interval (Smith and Botha-Brink, 2014).

1.2.1.3. Lithofacies association C. The third lithofacies association was introduced first by Ward et al. (2000) and subsequently associated by many with the PTB, itself. It is described as a laminated mudrock interval, three to five meters in thickness (Smith and Ward, 2001; Ward et al., 2005; but also see Retallack et al., 2003; Coney et al., 2007; Botha-Brink et al., 2014) that consists of dark reddish–brown (2.5YR 3/4; 2.5YR 2.5/4) and olive–gray (5Y 5/2; Smith and Botha, 2005; Botha and Smith, 2006) siltstone-mudstone couplets, each 1–3 cm thick (Smith and Ward, 2001; Smith and Botha-Brink, 2014). These very thin beds have a sharp, flat basal bounding surface, fine upwards (Smith and Botha-Brink, 2014), and are reported to contain very thin laminae (i.e., light-dark alterations) interpreted as varves (Retallack et al., 2003; Smith and Botha, 2005). Their upper surfaces commonly display oscillation ripples and textures reminiscent of algal mat impressions (Smith and Botha-Brink, 2014). Smith and Botha-Brink (2014) considered a single horizon of large brown weathering calcareous nodules, now reported from the top of this interval (Smith and Botha, 2005), to represent a workable lithological marker of the End- Permian in the southern Karoo Basin. Lithofacies Association C has been considered unique, with rooting structures, *Katbergia* burrows, and the presence of nodules being the only evidence of pedogenesis. In addition, Retallack et al. (2003) described a 10-cm-thick claystone breccia from the laminated interval, but the presence of this facies has never been corroborated by subsequent publications. A dearth of vertebrate remains recovered from this facies association led previous workers to place the PTB at the base of this interval (Smith and Ward, 2001; Ward et al., 2005). Subsequently, the vertebrate-defined PTB was moved to the top of this lithofacies association when prospecting yielded an impoverished *Daptocephalus* AZ in this interval. Lithofacies C is in the lower few meters of the Palingkloof Member at Bethulie.

The appearance of lithofacies association C has been termed an “event” by various workers (Smith and Ward, 2001; Retallack et al., 2003; Ward et al., 2005; Smith and Botha, 2005; Smith and Botha-Brink, 2014) and the characteristics of this interval have been used by many as the definitive PTB marker (Viglietti et al., 2016; Rubidge et al., 2016). The “event bed”, described at Bethulie, Lootsberg Pass, and other localities was not, initially, used in a time connotation. Rather, it was used to describe a rapid and widespread environmental change, which Ward et al. (2005) correlated, using bio-, magneto- and chemostratigraphy, with the global PTB (Ward et al., 2012). Gastaldo et al. (2009) were unable to trace this lithostratigraphic unit at the same stratigraphic level across a < 1 km distance at Bethulie. Their field data developed in a stratigraphic framework resulted in a rejection of the boundary-bed concept, which continues to be debated (Ward et al., 2012; Gastaldo and Neveling, 2012) but propagated in the literature (Smith and Botha-Brink, 2014; Botha-Brink et al., 2014, 2016; Viglietti et al., 2016).

1.2.1.4. Lithofacies association D. Overlying the reported Last Appearance Datum of the *Daptocephalus* AZ in Lithofacies Association C is an interval of siltstone characterized by massive maroon and olive-gray siltstone, in which the *Lystrosaurus* AZ fauna is preserved. Lithofacies association D contains minor thin-gullied sandstone sheets (Smith and Ward, 2001; Smith and Botha, 2005: Botha and Smith, 2006; Smith and Botha-Brink, 2014; Botha-Brink et al., 2014) without the reported presence of fluvial channel-form bodies. A greater abundance of desiccation features and a slightly lighter color (2.5 YR 3/6), when compared to the dark reddish brown (2.5 YR 2.5/4) of the previous facies, are reported as criteria on which to recognize it. At Bethulie, it is illustrated to be nearly 50 m thick (Smith and Botha-Brink, 2014; their Fig. 3) and encompasses the upper part of the Palingkloof Member and ~10 m of the lowermost Katberg Formation.

1.2.1.5. Lithofacies association E. The boundary interval is capped by the sandstone-dominated Katberg Formation. The Katberg Formation is composed of vertically stacked and multi-storied (5–10 m thick) tabular, olive-gray to grayish-yellow, fine- to medium-grained sandstone bodies separated by intervals of light olive-gray and dark-red mudstones (Ward et al., 2000; Smith and Ward, 2001; Ward et al., 2005; Smith and Botha-Brink, 2014). A distinctive feature of these sandstones is the common occurrence of irregular disconformities, lined with lenses of intraformational conglomerates composed of mud

pebbles, reworked bone fragments, and numerous spheroidal pedogenic pisoliths that may exhibit internal septarian shrinkage cracks (Botha and Smith, 2006; Smith and Botha-Brink, 2014). These sandstone bodies, in which elements of the *Lystrosaurus* AZ fauna are found, are interpreted to represent deposition in wide, shallow low-sinuosity, "braided" rivers (Ward et al., 2005; Smith and Botha-Brink, 2014).

1.2.2. Biostratigraphy

As often is the case, as field collection of new fossils continued, biostratigraphic ranges were refined allowing Smith and Ward (2001) to first extend the range of the genus *Lystrosaurus* downward, overlapping the *Daptocephalus* AZ by > 41 m (recall that Hotton, 1967 first reported the biostratigraphic range overlap at Lootsberg Pass). Subsequently, Botha and Smith (2007) proposed that the majority of these lower occurrences of *Lystrosaurus* can be assigned to the species L. *maccaigi* and that this taxon was restricted to the *Daptocephalus* AZ. It must be noted, though, that when Kammerer et al. (2011) re-examined this L. *maccaigi* in museum collections, they only could find six specimens that conformed to the species diagnostic criteria. Most specimens lacked the diagnostic features to be assigned to the species L. *maccaigi* under their typological approach.

The co-occurrence of L. *maccaigi* with *Daptocephalus* (*Dicynodon*) *laceriteps*, as reported by Smith and Botha-Brink (2014), was continued by Viglietti et al. (2016) who consider this species to be the index taxon of the Upper *Daptocephalus* AZ. A second species of *Lystrosaurus*, *L. curvatus*, is reported to have a restricted biostratigraphic range. This taxon occurs in the uppermost *Daptocephalus* and basalmost *Lystrosaurus* AZs. Based on the overlap of an additional three taxa (*Moschorhinus*, *Tetracynodon*, *Ictidusuchoides*) with *Lystrosaurus curvatus* and other *Lystrosaurus* AZ fauna, Smith and Botha (2005) distinguished between extinction, survivor, and recovery faunas (see Gastaldo et al., 2017, for a test of this hypothesis). The composition of the survivor taxa have changed, following taxonomic and stratigraphic revision (Smith and Botha-Brink, 2014; Viglietti et al., 2016), with a decrease in number (see Lucas, 2017a). Yet, vertebrate ranges still are considered sufficient for the identification of three extinction and one "early recovery" phases in the boundary interval.

1.2.2.1. Taxonomic considerations and assemblage-zone designations. There exists continued debate among vertebrate paleontologists about the systematic assignment of several late Permian taxa used to circumscribe the *Daptocephalus* (*Dicynodon*) AZ, a debate that is germane to the current study. Kitching (1971, 1977) was the first to circumscribe the *Daptocephalus* Zone which was renamed, shortly thereafter, as the *Dicynodon lacerticeps* AZ by Keyser and Smith (1978). These authors considered *Daptocephalus* to represent a junior synonym of *Dicynodon lacerticeps* and later researchers, following the scheme in Rubidge (1995), referred to the *Dicynodon* AZ in subsequent PTB studies (Smith, 1995; Ward et al., 2000, 2005; Smith and Botha-Brink, 2014). Kammerer et al. (2011) undertook a comprehensive taxonomic revision of these taxa, resurrected the genus *Daptocephalus*, and identified an additional nine genera in the complex. They concluded that *Dicynodon* sensu *strictu* ranged across the *Cistecephalus* and *Dicynodon* AZs, whereas only *Daptocephalus* was restricted to the *Dicynodon* AZ. With this biostratigraphic model in mind, Viglietti et al. (2016) reassessed the stratigraphic range of *Dicynodon*, incorporating the data in Smith and Botha-Brink (2014) (but see Gastaldo et al., 2017), redefined the *Dicynodon* AZ as the *Daptocephalus* AZ, and subdivided it into lower (co-occurrence of *Dicynodon* and *Daptocephalus*) and upper (co-occurrence of *Daptocephalus* and *Lystrosaurus maccaigi*) intervals. Currently, *Lystrosaurus maccaigi* is considered to be restricted to the upper *Daptocephalus* AZ and absent from the overlying *Lystrosaurus* AZ (Smith and Botha, 2005; Botha and Smith, 2007; Viglietti et al., 2016). Not all authors agree on the subdivision of the genus *Dicynodon*.

Lucas (1997, 2006) follows the use of the genus *Dicynodon* in the sense of Cluver and Hotton (1981) and, recently, rejected the generic subdivision of taxa (Lucas, 2017b) proposed by Kammerer et al. (2011). He cites several reasons why the genus *Dicynodon* should be retained for all taxa split by these authors. Lucas (2017b) contends that Kammerer et al.'s (2011) typification of taxa did not account for a range of morphological variation inherent in any population of specimens, even from collections made at a single locality, nor did it include any analysis of an ontogenetic series of skulls. Rather, Kammerer et al. (2011) focused on holotypes of species assigned to the genus from which four skull morphotypes–*Dinanomodon*, *Daptocephalus*, *Dicynodon*, and *Basilodon*–could be discerned. The only morphometric data provided by Kammerer et al. (2011), though, was used to differentiate the snout shape between *Dicynodon lacerticeps* and *Daptocephalus leoniceps* (see Gastaldo et al., 2017). Lucas (2017b) contends that the separation of taxa also is unjustified in the absence of any suite of morphometric data and analyses. For example, Kammerer et al. (2011) based one new skull morphotype on an incomplete skull of *Basilodon*, which leaves questions about how extensive a character suite can be compiled under these circumstances. And, Lucas (2017b) raises a serious concern about how Viglietti et al. (2016) could assign jaw, skull, and other incompletely preserved specimens to *Daptocephalus* when a nearly complete skull, in which the interorbital region and/or snout is well preserved, is what is needed to identify the taxon (Kammerer et al., 2011). The problem recently was compounded by the recovery of a nearly complete dicynodontoid skull by Gastaldo et al. (2017; AM4757) in the upper *Daptocephalus* zone near Old Lootsberg Pass. Initially, Kammerer (pers. comm. 9/2013) identified this skull (Gastaldo et al., 2017, Fig. 12) as *D. lacerticeps* while visiting The Albany Museum. Subsequently, after reviewing his notes, Kammerer (pers. comm. 9/2016) remarked that the specimen displayed "a problematic mixture of *Dicynodon and Daptocephalus* characters" and placed it into *Daptocephalus* although acknowledging that it could also represent an extremely large *Dicynodon* (Gastaldo et al., 2017, p. 358). Although there are unquestionable problems with the current status of these fossils and, therefore, the name placed onto the vertebrate assemblage zone in which they occur, we have maintained the current paradigm. All the references to the *Daptocephalus* AZ henceforth include references to the *Dicynodon* AZ by previous workers.

1.2.3. Palaeoenvironmental extinction model

Smith (1995) interpreted a change in the fluvial environment, from meandering channel to "braided" architectures, to be coincident with the vertebrate turnover which, at the time, was thought to be the result of tectonics affecting the basin. A switch occurred from a Karoo landscape dominated by alluvial plains traversed by a few large, highly meandering rivers (Lithofacies A) to a distributary channel network that eventually widened and separated into a braided pattern (Lithofacies D). The changeover is envisioned to have occurred through a transitional stage when the rivers straightened and branched (Lithofacies B), with braidplains developed in response to increased sediment load from the Cape Fold Belt. Later, Ward et al. (2000) discarded the role of basin tectonics in the sedimentological change across the Balfour–Katberg formational contact because they could not identify an appropriately dated paroxysm in the Cape Fold Belt (Hälbich, 1983; Gresse et al., 1992). As an alternative, they proposed that the fluvial change was the result of a dramatic increase in sediment load caused by widespread vegetation die-off in response to regional drying and drought. Based on the change in fluvial style and reddening of floodplain soils, supported by vertebrate taphonomic data, Smith and Ward (2001) considered the boundary interval to reflect increased aridification. This interpretation is retained by subsequent workers (e.g., Smith and Botha, 2005; Coney et al., 2007; Smith and Botha-Brink, 2014; Rubidge et al., 2016; Viglietti et al., 2016). But not all previous workers were in agreement.

In contrast, Retallack et al. (2003), using pedogenic data, proposed that the Permian palaeoclimate was strongly seasonal and arid in the

latest Permian and there was a shift to a less seasonal, semi-arid to subhumid Triassic paleoclimate. In part, the interpretation was based on the depth to pedogenic calcic horizons in all paleosols with nodules, regardless of whether calcite precipitated in equilibrium with atmospheric gas pressures or as a result of microbial decay of organic matter (Tabor et al., 2007). This paradigm was reviewed by Smith and Botha, 2005 (Botha and Smith, 2006) who considered the increased depth to pedogenic calcic horizon and introduction of sandstone sheets, which display basal gulleying draped by lenses of intraformational conglomerate containing pedogenic nodules, to be indicative of ephemeral discharge. Their explanation centered on an interpreted increase in mean annual temperature combined with the onset of a highly seasonal, but unreliable (monsoonal) rainfall regime. Together with an increased frequency of dessication features, rubification of soils, and vertebrate taphonomic data which included an increase in observed vertebrate-fossil articulation, increasing aridity into the Triassic was interpreted up-section (Smith and Ward, 2001; Smith and Botha, 2005; Botha and Smith, 2006, 2007). A new interpretation was proposed for the thick red siltstones above the *Daptocephalus–Lystrosaurus* biozone contact. Following Smith (1995), these rocks were believed to represent aeolian deposits and used to support the presence of a semi-arid climate, with a short, but intensive, wet season for the post-extinction landscape.

In general, current paleoclimate models for the Beaufort—Katberg transition mirror that first proposed by Smith (1995). An overall trend of increasing aridification, modified by Ward et al. (2005), envisions that a prolonged period of environmental stress (upper Elandsburg and lower Palingkloof Mbr.) was punctuated by a short interval of even greater perturbation (Lithofacies Association C) associated with biozone contact. In this context the "event bed" laminites were interpreted to represent turbidite deposition in playa lakes during a short period when the entire Karoo Basin was almost devoid of vegetation and that soil-forming processes had been suspended (Retallack et al., 2003; Smith and Botha, 2005; Smith and Botha-Brink, 2014). These unusual circumstances were interpreted to be the result of a catastrophic drought responsible for the demise of the *Daptocephalus* AZ, caused by CO2-induced aridification (Smith and Botha-Brink, 2014).

1.2.4. A problematic model

The current terrestrial PTB model for the Karoo Basin represents more than two decades of published research. This model is widely accepted and plays a central role in our global scale interpretation of extinction and recovery dynamics on land during and after the event (e.g., Benton and Newell, 2014; Roopnarine and Angielczyk, 2015; Botha-Brink et al., 2016). However, the litmus test for any hypothesis is whether the details that lead to a proposed model can be verified repeatedly by independent study. We have asserted (Gastaldo et al., 2005, 2009, 2015, 2017; Gastaldo and Neveling, 2012, 2016; Neveling et al., 2016a, 2016b) that many aspects of the model are not repeatable, raising questions about the validity and utility of the terrestrial end-Permian extinction model for Karoo Basin successions. The reader is directed to these publications for our observations, data, and a more extensive discussion of problems inherent in the current paradigm. The following section focuses on the assertion of a unique event bed that can be used as a time marker, the PTB, that can be mapped across the basin (Smith and Botha-Brink, 2014; Botha-Brink et al., 2014).

1.2.4.1. Playa Lake deposition at the vertebrate-defined PTB. Smith and Ward (2001) used what they believed to be a unique lithofacies, which Ward et al. (2005) designated as their Unit III and Smith and Botha-Brink (2014) termed their Lithofacies Association C, to mark the stratigraphic position of the vertebrate turnover and, hence, the inferred Permian–Triassic Boundary (PTB). The characteristics of this 3- to 5-m-thick, rhythmically bedded, interlaminated interval first were reported to consist of alternating olive-gray and dark reddish-brown (Smith and Ward, 2001) but, more recently, of reddish-brown siltstone/mudstone (Smith and Botha-Brink, 2014) couplets. These workers, and others, have used this lithofacies as a correlation datum (Ward et al., 2005; Botha-Brink et al., 2014), claiming that it is a basin-wide mappable unit (Smith and Botha-Brink, 2014), and having reported it to extend into Antarctica (Retallack et al., 2003). These claims are in spite of empirical field evidence to the contrary presented by Gastaldo et al. (2009) and Gastaldo and Neveling (2012, 2016). In these contributions, they demonstrated that the lithofacies is neither unique nor can be traced along 1 km of transect at the same stratigraphic position at Bethulie. This fact subsequently was acknowledged by Ward et al. (2012), who admit that the lithofacies is non-unique in its stratigraphic distribution. Yet, the interlaminated lithofacies, the interpretation of which has changed over time, continues to be used as a reliable lithologic criterion on which to identify the upper contact (stratigraphic top) of the *Daptocephalus* AZ and, as such, the vertebrate-defined PTB in the Karoo Basin (e.g., Botha-Brink et al., 2014; Viglietti et al., 2016) and globally (Benton and Newell, 2014; Rey et al., 2016).

Smith (1995) was the first to recognize a changeover in paleosol features from the *Daptocephalus* (*Dicynodon*) AZ to the *Lystrosaurus* AZ at Bethulie, wherein drab, greenish-gray Entisols, Calcic Vertisols, and Gleysols in the former were replaced by well developed Calcisols of a reddish-gray (rubified) color. This changeover is reported to have been rapid, occurring just prior to the assemblage-zone boundary contact, and interpreted to have been the result of a regional lowering of watertable as a consequence of increasing aridity. Smith (1995) makes no mention of any unique succession at the Bethulie locality, a feature that appears in subsequent publications.

An interlaminated facies associated with the PTB is first introduced by Ward et al. (2000) and reported to be unique at seven localities in which the vertebrate-defined boundary occurs. They describe the transitional succession as a sandstone-shale unit of several meters thickness, underlain by fluvial channel architectures interpreted to represent meandering channel deposits and overlain channel architectures interpreted as braided river systems. The changeover in fluvial architectural styles was attributed to increasing aridity, the demise of the terrestrial flora, and increasing sediment load as a consequence of increased erosion. Subsequently, the significance of the transitional deposits was developed further.

The presence of a unique "event bed" was proposed by Smith and Ward (2001) for the transitional deposits at Bethulie and Old Lootsberg Pass (see Gastaldo et al., 2009, 2017). The PTB being placed at the base of the unit at the time. The "event bed" was characterized as a 3–5 m interval of "distinctively laminated maroon mud rock made up of thinly bedded dark reddish-brown and olive-gray siltstone-mudstone couplets" (Smith and Ward, 2001, p. 1148) and claiming a coincident FAD of a callianassid-shrimp burrow (= *Katbergia*; Gastaldo and Rolerson, 2008). The explanation for the "event bed" conforms to that proposed by Ward et al. (2000) as part of the transition in fluvial architectural styles in response to increasing aridity. Neither in these papers, nor in Ward et al. (2005, their Unit II), is a depositional environment interpreted for this interlaminated interval. That same year, Smith and Botha (2005), restated verbatim in Botha and Smith (2006), report new features of the interval based, in part, on its characterization in Retallack et al. (2003).

The "event bed" of Smith and Ward (2001) had been recast as a laminite interval by Retallack et al. (2003), who describe them as purple to gray beds with a thickness up to seven meters. Retallack et al. (2003) are the first to place a playa-lake interpretation on the laminite interval using the presence of varve-like lamination, crustacean (= *Katbergia*; Gastaldo and Rolerson, 2008) burrows, algal stromatolites, and vertebrate trackways as evidence of periodic drying. Although this interpretation appears not to have been adopted by Ward et al. (2005), Smith and Botha (2005) promote this interpretation when they describe the regionally extensive interval as consisting of at least 5 m of maroon colored, thin and rhythmically bedded laminites. In their description, they add a single horizon of large calcite-cemented nodules as a defining feature in most sections (see Gastaldo et al., 2009). The

laminites are described as consisting of couplets of centimeter-scale, dark reddish–brown siltstone overlain by olive–gray mudstone, although grain-size characteristics of what constitutes a siltstone versus a mudrock are not provided (= clay; Smith and Botha-Brink, 2014). Differences in color of the laminites were ascribed to sediment alteration in response to dolorite heating (see below). Primary sedimentary structures reported at the contact between siltstone and mudstone include oscillation ripples and textures resembling algal mats (= stromatolites of Retallack et al., 2003). Smith and Botha (2005, p. 627) found no evidence of pedogenesis, although Retallack et al. (2003) report weak pedogenic alteration, and interpret them to represent a body of "shallow standing water with periodic sub-aerial exposure and desiccation." Collectively, the reported features of the interval are used as evidence to suggest that this was a synchronous, basin-wide facies representing a thermally stratified playa lake setting. This interpretation is reinforced in Smith and Botha-Brink (2014) in a brief comparison with a reported similar facies in Russia (Newell et al., 2010).

1.3. Purpose

The current study is designed to review and test the interpretation of Retallack et al. (2003), Smith and Botha (2005), Botha and Smith (2006), and Smith and Botha-Brink (2014) for the stratigraphic succession they identify as an extensive playa lake deposit on the Bethel Farm, near Bethulie, Free State, separating different fluvial regimes. We take a multidisciplinary approach using detailed measurements of lithostratigraphy and facies relationships, petrography, major- and trace-element geochemistry, Mössbauer spectroscopy, and rock magnetic data to evaluate this lithofacies and surrounding rocks. Our data are compared with criteria developed for the recognition of Permian playa deposits in Europe and modern regimes. We conclude that there is no evidence to support the interpretation of Smith and Botha-Brink (2014) that this interval represents a playa setting. In addition, we do not find any evidence to support an aridification trend in this part of the Beaufort Group, adding support to the conclusions drawn by Li et al. (2017) at Old Lootsberg Pass in the Eastern Cape Province. Rather, physical and chemical evidence support an interpretation of prevailing wet conditions at the time when these sediments were deposited.

2. Locality

The "Bethulie locality" is located 30 km east of the town of Bethulie, on the farms Bethel 763, Heldenmoed 677, and Donald 207 (encompassing the farm Fairydale; Fig. 2). It is a well-known and productive fossil locality at the base of a deep valley that was discovered by James Kitching in 1977 (Abdala et al., 2006). Smith (1995) published the first stratigraphic log from the locality in which the PTB was interpreted, and his measured section is featured prominently in subsequent publications (Ward et al., 2000, 2005; Smith and Ward, 2001; Botha and Smith, 2006, 2007; Smith and Botha-Brink, 2014). It is arguably the most important PTB locality in South Africa, having yielded the largest number of vertebrate fossils of any section studied, to date (~250 fossils – see Smith and Botha-Brink, 2014, their Supplementary data).

3. Methods

3.1. Field methods

Lithologic sections of various thickness were measured using a Jacob staff with Abney level across the Bethel and Heldenmoed farms, allowing for the development of a lithostratigraphic framework (Neveling et al., 2016a). The current report focuses on the sedimentary rocks directly below, inclusive of, and directly above Smith and Ward's (2001) "event bed" exposed on these farms (S 30.41843°, E 026.26761° WGS 84; Fig. 3) where they were described using standardized methods. Field methods include the use a Sand-gauge grain-size chart (W.F. McCollough, MD) and hand lens for comparative purposes, and a Munsell Rock-Color Chart for color characterization. The stratigraphic interval encompassing Facies C of Smith and Botha-Brink (2014, p. 103–104)—the interlaminated boundary interval—was trenched to ground level using a pickaxe, and fresh exposures were described on a cm-basis. Representative beds were photographed against a Munsell Color Chart, and competent hand samples collected for thin sections (prepared by Applied Petrographic Services Inc.). Facies relationships were assessed by walking the upper contact (bounding surface) of the reported interlaminated interval (see below) along strike to the southeast and northwest for a total lateral distance of > 650 m (see Supplemental data Table 1). Short stratigraphic sections were measured where lithofacies changes were noted, allowing for the development of an understanding of the interval's lateral profile. Representative hand samples also were collected for geochemical analyses.

We have sampled the Bethulie locality extensively for paleomagnetic purposes and, thus, magnetic polarity stratigraphy information. Six relatively thin (0.5 to 2.0 m wide) dolerite dikes are exposed in the area near the inferred "event bed." Excellent exposures of these dikes and their thermally modified (to contact metamorphosed) host-contact strata are typical in the dongas (erosional gullies). Samples were collected from competent fine-grained sandstone-and-siltstone intervals by drilling oriented cores using a portable field drill with a non-magnetic diamond drill bit. Typically, seven to 12 + independently-oriented core samples have been obtained from each suitable bed. Most sampled beds are exposed in the main donga adjacent to and/or contained in Smith's (1995) measured section (see Supplemental data). For the current study, our rock magnetic measurements utilized splits of the powdered samples used for geochemical investigations.

3.2. Geochemistry and mineralogy

Techniques used to characterize geochemistry and mineralogy include bulk elemental composition obtained using X-ray fluorescence (XRF) and X-ray diffraction (XRD) for clay mineralogy. Because XRF data do not discriminate oxidized and reduced forms of Fe, selected samples were analyzed using Mössbauer spectroscopy. Once the presence of finely dispersed hematite was confirmed by this technique, the distribution and morphology of hematite grains were assessed with scanning electron microscopy (SEM), and elemental composition confirmed using EDS.

3.2.1. Elemental composition by XRF and glow discharge mass spectroscopy

Elemental composition of areas displaying a homogenous matrix in seven thin sections of siltstone and the clay fractions of four siltstone samples were obtained using a Bruker M4 Tornado Micro-XRF spectrometer. Data were analyzed with the M4 Tornado analytic software (ver. 1.2.0.2687). For each thin section, three to eight field-of-view-sized regions were marked on the slide under 100 × magnification, with the highest numbers selected for samples displaying greater lithologic heterogeneity where greater geochemical variation was likely based on pilot-project data. Data were acquired from 40 to 71 sampling points per thin section, manually chosen in the Micro-XRF under 100 × magnification. The clay fraction (< 10 μm) of four samples was separated after removal of any iron oxyhydroxide staining on weathered samples before powdering. These were hand ground to powders using a mortar and pestle and made into clay slides using the modified Drever's filter-membrane peel technique by Pollastro (1982). Data were acquired from an average of 40 sampling points per slide, manually chosen in the Micro-XRF under 10 × magnification. All samples were run for the region between 0.25 keV and 20.00 keV, with a live time of 30 s per sampling point (30 μm). The following elements were quantified: Si, Al, K, Fe, Na, Mg, Ca, Ti, Mn, P, and S.

Two hand samples, one olive-gray and the other grayish-red, collected from the interlaminated unit figured by Gastaldo et al. (2009, their Fig. 2), and referred to as demonstrable of the PTB "event beds" by

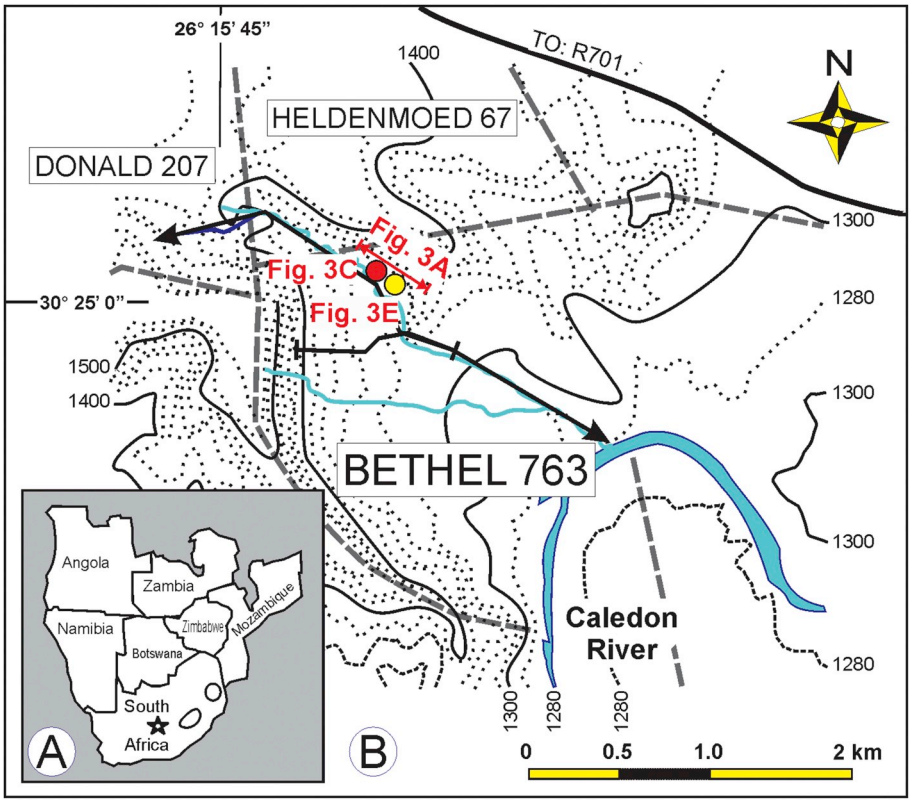

Fig. 2. Locality maps. (A) Map of southern Africa on which Bethulie is located with a star. (B) Map of the Bethel 763, Heldenmoed 67, and Donald 207 farms localities in the Free State on which outcrop of the vertebrate assemblage zone boundary is exposed and described by Smith (1995), Gastaldo et al. (2009), Smith and Botha-Brink (2014), and Neveling et al. (2016a). Solid line with arrows at the ends marks the erosional gully (donga) in which measured stratigraphic sections of Smith and Botha-Brink (2014) and Neveling et al. (2016a) occur. The site figured by Smith and Botha-Brink (2014) (their Fig. 5) as their PTB on the Bethel Farm was trenched at red-filled circle corresponding to Fig. 3B, and laterally equivalent facies corresponding to samples recovered at Fig. 3E is indicated as a yellow-filled circle. (For interpretation of the references to color in this figure legend, the reader is referred to the web version of this article.)

Smith and Botha-Brink (2014, p. 103), were sent to Northern Analytical Laboratory, Inc., Londonderry, New Hampshire. A full suite of major, minor, and trace elements were analyzed by Glow Discharge Mass Spectroscopy (see Supplemental information).

The clay mineralogy of four samples, two greenish-gray (BS 7.5, BS 7.8) and two grayish-red (BS 7.4, BS 7.6; Fig. 4) siltstone, was analyzed at Southern Methodist University following the methods in Li et al. (2017). Data are for oriented < 2 μm aggregates and powder mounts.

3.2.2. Fe^{2+}/Fe^{3+} concentrations by Mössbauer spectroscopy

Two samples, one grayish-red (BS 7.6) and one olive-gray (BS 7.11), from the trenched section were powdered, sieved, and sent to Mount Holyoke College for Mössbauer spectroscopic analysis (analytical methods employed can be found in Supplemental data; see Li et al., 2017). These were chosen on the basis of representative sample color, comparable grain size, and stratigraphic position in Facies C of Smith and Botha-Brink (2014). Sample BS 7.6 is a grayish-red siltstone at the uppermost contact of the reported interlaminated unit, whereas BS 7.11 was collected from the same stratigraphic position 180 m to the southeast (Fig. 4).

3.2.3. Thin section SEM imaging

SEM imaging was undertaken at the University of Maine-Orono. The sample confirmed to have hematite by Mössbauer spectroscopy was scanned using a Tescan Vega II XMU tungsten filament SEM with backscatter capabilities to determine the distribution and morphology of metal-rich oxides and silicates. Thin sections were carbon-coated before scanning, and mineralogy was determined based on semi-quantitative elemental composition data obtained by the EDAX Pegasus EDS system. Digital images and EDS X-ray point spectra of representative grains were collected.

3.2.4. Total organic carbon and nitrogen

Powdered whole-rock samples of the greenish-gray and grayish-red lithologies were analyzed for Total Organic Carbon and Nitrogen using a Perkin-Elmer 2400 Elemental Analyzer. Samples were pre-treated with HCL to remove any carbonate prior to analysis; all samples were devoid of carbonate. Acetanilide was used as the standard with the following known values: Carbon 71.09%, H 6.71%, and N is 10.36%.

3.3. Rock magnetic measurements

Disaggregated samples were packed into appropriate non-magnetic containers (either 7 cm^3 IODP plastic boxes or size 04 gelatin capsules) for most magnetic measurements. Measurements included bulk magnetic susceptibility (using an AGICO Kappabridge KLY-3S instrument), stepwise acquisition of an isothermal remanent magnetization (IRM) up to a field over 3.0 Tesla (T), backfield direct field demagnetization (using an ASC multi-coil impulse magnet with measurements on an AGICO JR5A spinner magnetometer), and magnetic hysteresis parameter determinations using a Princeton Measurements Corporation vibrating sample magnetometer (VSM). For the hysteresis parameter determinations, two small rock fragments from each sample (few 100 mg) were used for VSM measurements. Finally, we monitored the bulk susceptibility of small quantities (500–600 mg) of powdered samples as a function of heating to 640 °C and subsequent cooling using an AGICO CS4 apparatus interfaced with an AGICO MFK1-A susceptibility system. These experiments were carried out in an argon atmosphere and always involved at least two heating/cooling cycles, to better investigate potential changes in magnetic mineralogy as a function of heating.

3.4. Data analyses

Descriptive statistics and bivariate plots (Sheldon and Tabor, 2009) were constructed using XRF whole rock and clay fraction data. The Komologorov-Smirnov test was run to determine whether mean concentrations of major elements from greenish-gray and grayish-gray samples were distributed normally. No whole-rock sample distribution conformed to a normal distribution. Hence, the non-parametric Mann-

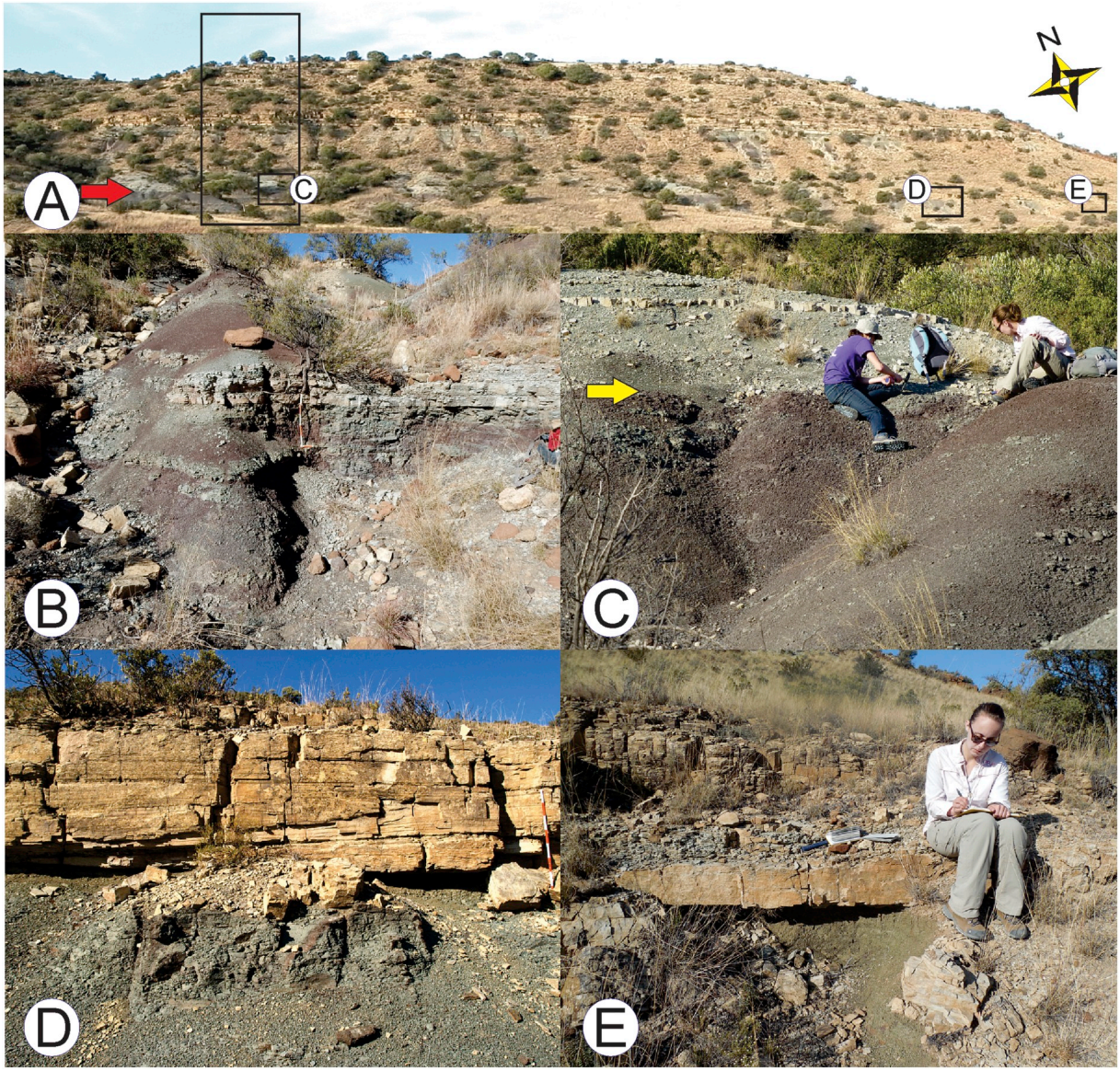

Fig. 3. Site on the Bethel Farm where the vertebrate-defined PTB occurs with images of the succession physically traced to the northwest and southeast. (A) Panoramic view of the hillside on which the vertebrate defined PTB is located. Arrow points to the top of what Smith and Botha-Brink (2014) report as an interlaminated unit–Facies C–where vertebrate turnover from the *Daptocephalus* to *Lystrosaurus* AZ marks their boundary (marked as 0 [PTB], Smith and Botha-Brink, 2014, their Fig. 12) against which the stratigraphic position of vertebrates collected on the farm are compared. Large rectangle outlines the position of Smith and Botha-Brink's (2014) (their Fig. 5) image (Fig. 4); smaller rectangles are images of laterally equivalent beds traced physically across the outcrop in the following images. (B) Outcrop traced to the northwest (S30.41706°, E026.26679° WGS 84) demonstrating a change in the character of the reported laminated interval illustrated in C. Scale in dm. (C) Outcrop exposure of Smith and Botha-Brink's (2014) interlaminated interval (S30.41843°, E026.26761° WGS 84) with yellow arrow marking the contact of the unit with an overlying light olive gray siltstone. (D) The same bed physically traced 160 m to the southeast (S30.41982°, E026.26805° WGS 84; see Fig. 4) wherein the siltstone is predominantly olive gray with reddish gray mottling with a massive appearance, overlain by a thin, lenticular, crossbedded wacke. Scale in dm. (E) Outcrop exposure 220 m to the southeast (S30.42033°, E026.26808° WGS 84) where the reported interlaminated unit is a massive, olive gray siltstone beneath the lenticular wacke figured in (D).

Whitney *U* test was used to compare elemental data between the two siltstone suites.

4. Results

4.1. Lithostratigraphy and facies relationships

4.1.1. Identification of the stratigraphic position of Bethulie's "event bed"

The figured site at which Smith and Botha-Brink (2014, their Fig. 5) place the boundary between the *Daptocephalus* (formerly *Dicynodon*; Viglietti et al., 2016; although see Lucas, 2017a, 2017b who proposes a return to using the former designation) and *Lystrosaurus* AZ's is found on the Bethel Farm (Figs. 2, 3) and is unmistakable. It is a well exposed, southwest-facing, prominent interval of "rubified" reddish-brown (maroon) siltstone overlain by light olive-gray siltstone (Fig. 3A, C). This interval has been characterized in several ways in published reports. What appears to be the first mention of the "event" bed (Smith and Ward, 2001) is that of Smith (1995, p. 91), where he reports interchannel deposits of the *Lystrosaurus* AZ as comprised of "alternating beds of greenish silty sandstone and reddish-brown and green siltstone with minor mudstone veneers." Subsequently, Smith and Ward (2001, p. 1148) reiterated this field relation, describing the interval overlying their PTB as a "3–5 m of distinctively laminated maroon mudrock made up of thinly bedded dark reddish-brown and olive-gray siltstone-mudstone couplets." This characterization is maintained in Ward et al. (2005, p. 713), but the specific position of vertebrate turnover was

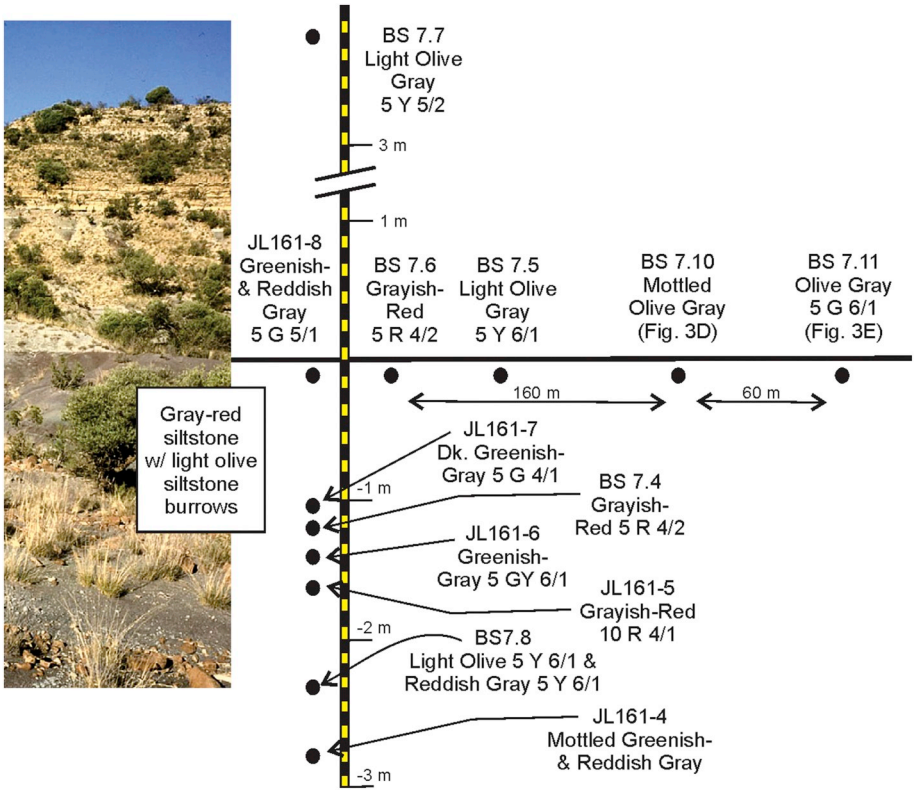

Fig. 4. Trenched unit of Fig. 3C with the upper contact of Smith and Botha-Brink's (2014) Facies C marked as 0 in the illustration, with competent samples from underlying (−) and overlying (+) beds indicated. Sample numbers are provided along with Munsell color designations for each. The grayish-red appearance of Facies C is the result of surficial overprinting by weathered fine siltstone with that color designation. The predominant color in Facies C is a variant of olive, greenish, or dark greenish gray. Photo from Smith and Botha-Brink (2014) (their Fig. 5) taken at the location outlined by large rectangle in Fig. 3. (For interpretation of the references to color in this figure legend, the reader is referred to the web version of this article.)

moved to the top of the event bed as described by Botha and Smith (2006, p. 504). In this publication, the interval was characterized as comprised of rhythmically laminated, maroon-colored mudrock, which also is illustrated (Botha and Smith, 2006, their Fig. 1). Subsequently, Smith and Botha-Brink (2014, their Fig. 5) characterize the same 3–5 m, event-bed interval (Facies C) as being dominated by maroon-colored, laminated mudrocks and provide another field photograph. Hence, there is no doubt that the succession we sampled on the Bethel Farm (Fig. 3A, C), and report upon herein, is the identical succession studied and characterized by these workers.

4.1.2. "Event bed" Lithostratigraphy and thin sections

On first impression, the exposure of Facies C of Smith and Botha-Brink (2014) (Fig. 5) where illustrated appears to be dominated by grayish-red siltstone because this fine-grained, weathered lithology actually veneers the exposure. When trenched, the true character of this sequence can be evaluated (Figs. 4, 5). This reported 3 + m thick interval consists of fining up beds, ranging from 20 to 40 cm in thickness, of sandy coarse or coarse siltstone (near the base) grading to fine siltstone (Fig. 5A). Most siltstone is of a greenish-gray hue (Figs. 4, 5) with subdominant hues of grayish-red; mottling of the two end members is common in the coarser fraction. Bed contacts are sharp between fine and overlying coarse siltstone, as well as between beds upsection where the succession loses any appearance of cyclicity. Here (i.e., − 1.1 m level in Fig. 5A), a 60-cm-thick bed of mottled to greenish-gray siltstone is overlain by mottled fine siltstone, the color of which varies laterally in the upper 30 cm of the section. In the field, little evidence exists for the presence of any primary structures exhibiting a consistent interlaminated (0–10 cm bed thickness; Tucker, 2011; Lisle et al., 2011) character, and no evidence exists for salt or gypsum pseudomorphs, calcretes, dessication cracks, or disruption structures. Small-scale ripples are present in well cemented, thin beds of greenish-gray and light olive-gray parts of the siltstone succession above the upper contact of this interval. Similar features are evident in thin sections.

The coarsest siltstone fractions exhibit mm-scale, low-angle cross-bedding (Fig. 5B, D) in a mottled (JL161-4) or dark greenish-gray (JL 161-7) lithology. Other samples appear homogenized, and this texture is common for both greenish-gray (BS 7.5) and grayish-red (BS 7.4) siltstone. Millimeter-scale mudchips are found at the top of the sampled interval only in grayish-red siltstone (BS 7.6; Fig. 5E); notably, greenish-gray samples at the same stratigraphic horizon exhibit no evidence of mudchips (BS 7.5; Fig. 5F). We find no evidence of halite or gypsum pseudomorphs or pyrite, nor any stromatolitic, fenestral, or disruption structures (Konrád et al., 2010) in any thin section. Although burrows are not exposed in the trenched outcrop, bioturbation is seen in thin section (JL161-7; Fig. 5D) as transverse sections of burrows.

4.1.3. Lateral facies relationships

The character of Smith and Botha-Brink's (2014) laminated "event" interval rapidly changes laterally over a few hundred meters of distance (Figs. 2, 6; Gastaldo et al., 2009; Gastaldo and Neveling, 2016; Neveling et al., 2016a; see Supplemental data). Traced from the trenched locality onto the Heldenmoed farm (Fig. 2), the interval transitions to beds of well-cemented, coarse greenish-gray siltstone overlain by grayish-red fine siltstone (Fig. 3B) near the farm's fence line. Farther to the northwest, this sequence is replaced by an interval featuring cm-scale beds of interlaminated sandy coarse siltstone grading into fine siltstone, both of which are range from mottled to predominantly greenish-gray in color (Fig. 6; Gastaldo et al., 2009, Fig. 2D). Gastaldo et al. (2009) reported primary and secondary structures from these exposures. The upper surfaces of cm-thick beds of more competent, and better cemented, sandy coarse siltstone may exhibit a range of features. These include wrinkle structures (Fig. 7A), ladder ripples (Fig. 7B), and interference ripple structures (Fig. 7C), depending on the stratigraphic position of the bed in outcrop. Primary structures are restricted to the lower half of the 2.5 m interval exposure where horizontal, silt-filled tubular burrows occur on some rippled surfaces (Fig. 7B at arrow). Higher stratigraphically, where greenish-gray, fine-grained siltstone becomes common in this interval, inclined parts of *Katbergia* (Gastaldo and Rolerson, 2008) burrows are encountered. When the "event bed" is

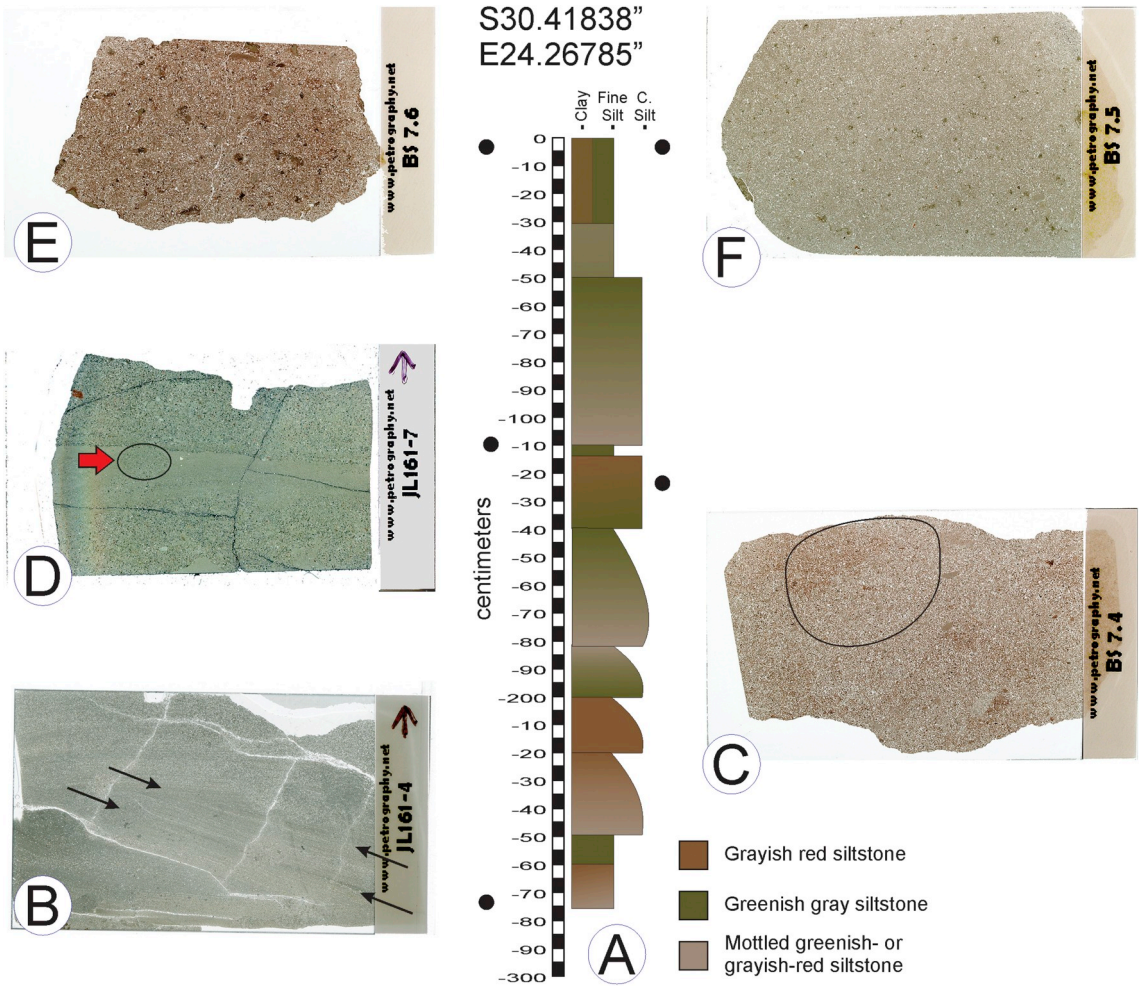

Fig. 5. Facies C measured with a Jacob staff and Abney level on a cm-scale and described following standard field protocols (see text). (A) Trenched and measured stratigraphic section of Facies C from which hand samples were collected and thin sections made (black filled circles). Stratigraphic distances measured from the top of the "Event Bed." Scale in cm. (B) Sample JL161-4 of a mottled greenish- and grayish-red siltstone near the base of Facies C in which finely laminated cross stratification is seen overlain by finely laminated planar beds exhibiting fining up features. (C) Sample BS 7.4 of a grayish-red coarse siltstone in which a faint elliptical burrow is outlined in a homogenized matrix. (D) Sample JL161-7 of a dark greenish-gray siltstone in which graded bedding occurs that is cross cut by a transverse burrow (in circle at arrow). An interval of fine siltstone occurs over a slightly coarser fraction. (E) Sample BS 7.6 taken below the upper contact of the interval in a grayish-red fine siltstone in which mm-scale mudchips are suspended in a matrix that appears homogenized. (F) Sample BS 7.5 taken below the upper contact (Fig. 3C) < 5 m to the southeast that is a light olive-gray fine siltstone. Similar to Fig. 5E, the sample is homogenized but with a lower proportion of mm-scale mudchips.

physically traced from the trenched section (Fig. 5) to the southeast, the character and color of this interval also changes (Figs. 3–5). A thin, planar yellowish-gray silty sandstone is in erosional and sharp contact with the interval 160 m distant, and this overlies a massive fine siltstone that is mottled in appearance (Fig. 3D). Physically traced to the southeast for a farther 60 m (Fig. 4), the siltstone becomes olive gray in coloration and appears massive (Fig. 3E). There is no evidence of grayish-red color in these latter exposures, having experienced a color gradation from grayish-red to mottled to greenish (olive) gray in < 250 m distance. Neither halite or gypsum pseudomorphs, calcareous cementation or calcrete horizonation, nor dessication features occur in any laterally equivalent interval.

4.2. Geochemistry

4.2.1. Major and minor elements

Major-element concentrations as determined by XRF are presented in Table 1 for both whole-rock and clay-fraction analyses, and each element is plotted against Fe (Fig. 8). The distribution of major-element values for most greenish gray and grayish-red whole-rock samples overlap, with greenish-gray BS 7.7 lying at the low end (average value 0.70%) and grayish-red BS 7.6 (average value 2.68%) lying at the high end of the Fe spectrum. Silica exhibits the highest range in values (ranging from 64.34–76.35%) followed by Al (13.73–20.38%). Average values of Ca, Na, and K reach maximum values of ~4.5%, whereas Mg values are < 1.8%, and Ti and Mn values are < 0.82% and < 0.07%, respectively.

There is a difference in the range of elemental values when whole-rock data and those of the clay fraction are compared. Major-element values obtained for the clay fraction of both greenish-gray and grayish-red siltstone show a tighter cluster in their distribution and overlap to a greater extent (Fig. 8). Most exhibit a limited distributional gradient with the exception of the Ca content in JL161-8 and Mn content of JL161-6, both of which are greenish-gray in color.

Results of the Mann-Whitney *U* test comparing the whole rock compositions of siltstone demonstrate that differently colored sample suites are indistinguishable (Table 1). *Z*-scores for each major element indicate that there is no statistically significant difference between greenish-gray to grayish-red siltstone in Facies C of Smith and Botha-Brink (2014) (Fig. 4). These data compare favorably with other reported geochemical data from the upper *Daptocephalus* AZ in other parts of the basin (Retallack et al., 2003; Coney et al., 2007; Gastaldo et al., 2014). Values obtained using Glow Discharge Mass Spectroscopy from greenish-gray and grayish-red siltstone for minor and trace elements

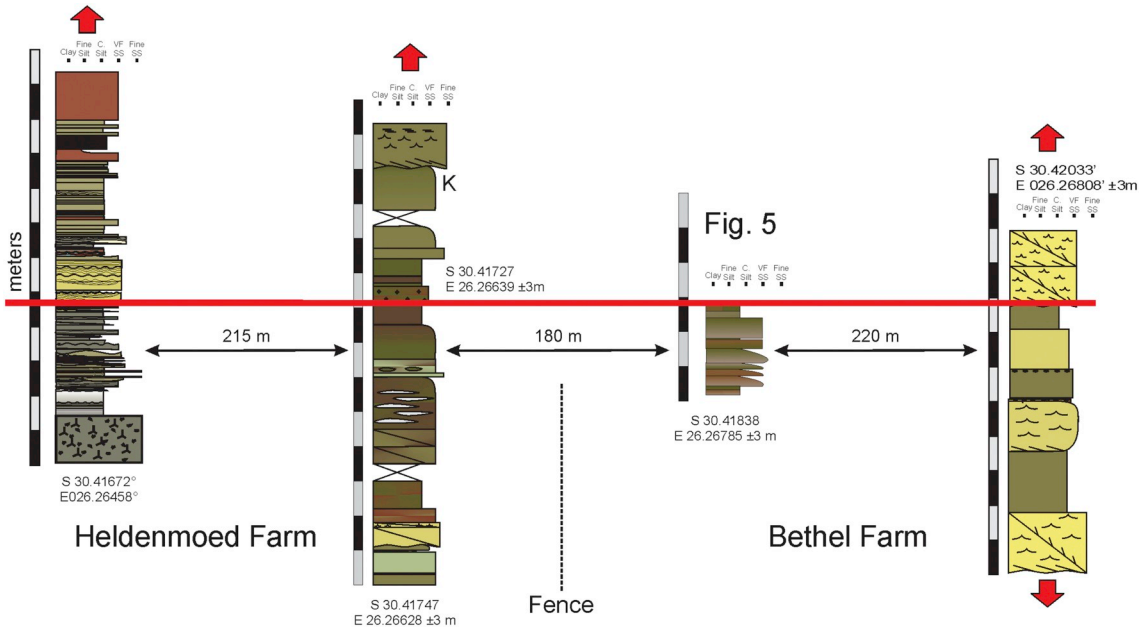

Fig. 6. Short, stratigraphic sections of four laterally equivalent intervals that were correlated physically along strike. The fence line between the Bethel and Heldenmoed farms is indicated (see Supplemental data for GPS, elevation, and locality data for descriptions of 20, laterally equivalent intervals traced along strike). Red arrows indicate measured sections above and below those illustrated. Scale in meters.

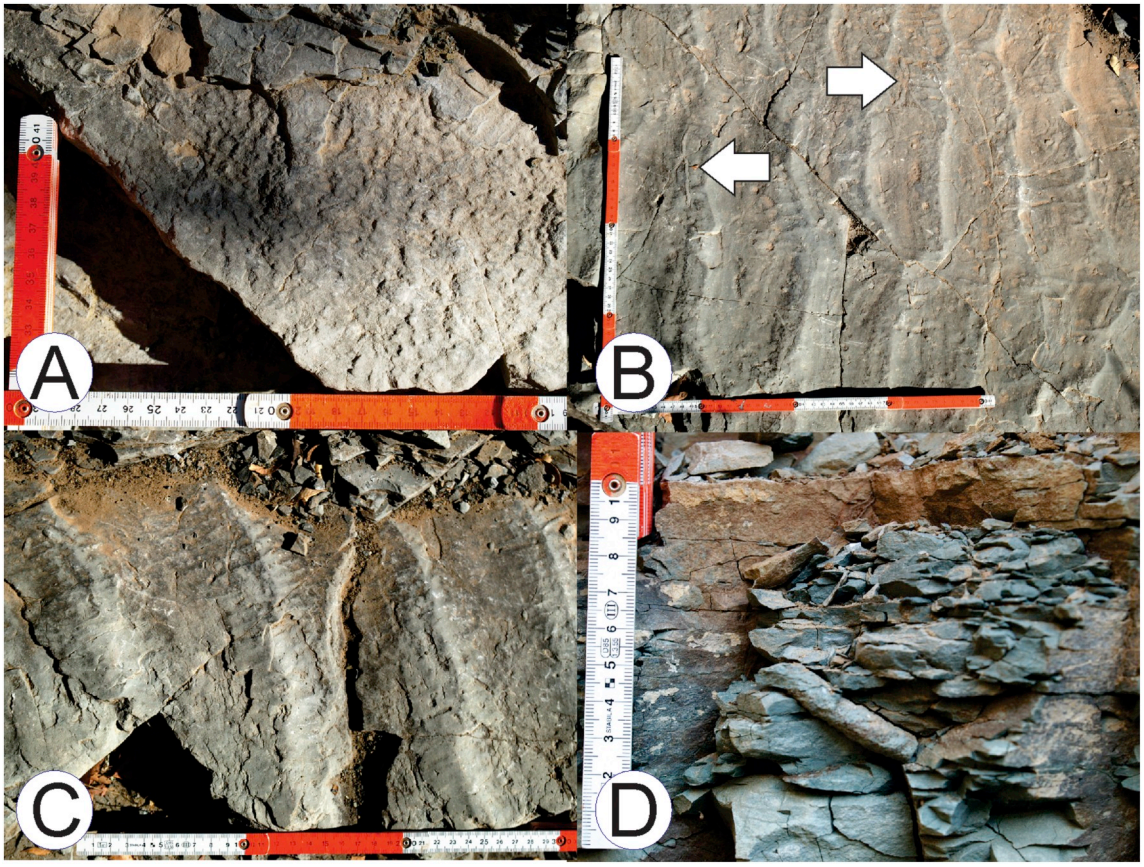

Fig. 7. Primary and biogenic structures preserved in Facies C exposed on the Heldenmoed Farm (Gastaldo et al., 2009, Fig. 2D). (A) Upper contact of a sandy coarse, cm-thick siltstone bed on which structures conforming to wrinkles are preserved. Scale in dm and cm. (B) Upper contact of coarse, cm-thick siltstone on which asymmetrical, ladder ripples and horizontal burrows conforming to *Planolites* are preserved (at arrows). Scale in dm and cm. (C) Upper contact of cm-thick coarse siltstone on which asymmetrical and interference ripples are preserved. Scale in dm and cm. (D) Inclined portion of a *Katbergia* burrow (Gastaldo and Rolerson, 2008) in the fine siltstone interval near the top of the succession. Scale in cm.

Table 1
Elemental concentrations obtained using XRF of Bethulie trenched samples. Komologorov-Smirnoff (K–S) D values test whether whole rock greenish-gray and reddish-gray sample data are normally distributed; no data set follows a normal distribution, resulting in the use of the non-parametric Mann-Whitney *U* test. Two tailed, Mann-Whitney *Z*-scores comparing greenish-gray and reddish-gray siltstones also show that there is no statistically significant difference between the two sample suites.

Sample	Na_2O	Std.Error	MgO	Std.Error	Al_2O_3	Std.Error	SiO_2	Std.Error	K_2O	Std.Error	CaO	Std.Error	TiO_2	Std.Error	MnO	Std.Error	FeO	Std.Error
BS 7.7	4.16	0.17	0.15	0.02	13.72	0.24	76.35	0.42	1.75	0.07	2.65	0.10	0.38	0.02	0.02	0.00	0.70	0.03
BS 7.5	2.15	0.11	1.11	0.19	15.12	0.23	72.56	0.71	3.91	0.13	1.71	0.22	0.66	0.04	0.05	0.01	2.34	0.43
JL161-6 (clay)	1.28	0.03	1.60	0.01	19.44	0.03	66.21	0.05	5.98	0.01	1.34	0.01	0.70	0.01	0.07	0.00	3.41	0.02
BS 7.11	2.48	0.12	0.96	0.04	16.12	0.24	71.11	0.47	4.41	0.13	2.59	0.25	0.45	0.05	0.03	0.00	1.57	0.08
JL161-7 (clay)	1.18	0.03	1.83	0.02	20.38	0.02	64.34	0.03	6.39	0.01	1.29	0.01	0.64	0.00	0.07	0.00	3.87	0.01
BS 7.8	3.15	0.16	0.98	0.03	15.62	0.45	69.18	1.38	4.04	0.08	4.65	1.49	0.59	0.02	0.04	0.00	1.34	0.04
JL161-4 (clay)	1.82	0.03	1.36	0.02	19.43	0.02	66.39	0.03	5.27	0.01	1.63	0.00	0.82	0.00	0.04	0.00	3.27	0.01
BS 7.10	2.89	0.14	0.94	0.04	15.89	0.26	71.43	0.43	4.17	0.10	1.91	0.08	0.53	0.03	0.03	0.00	2.02	0.09
BS 7.6	2.50	0.21	1.02	0.11	16.38	0.29	70.16	0.51	4.68	0.27	1.67	0.16	0.65	0.06	0.06	0.01	2.68	0.20
BS 7.4	2.72	0.12	1.04	0.03	16.36	0.21	70.61	0.35	4.40	0.09	1.85	0.08	0.63	0.03	0.04	0.00	2.19	0.06
161-8 (clay)	1.97	0.04	1.32	0.01	18.66	0.04	65.49	0.07	4.79	0.01	4.33	0.03	0.86	0.01	0.07	0.00	2.56	0.02
Average Sample suite	2.39	0.11	1.12	0.05	17.01	0.18	69.44	0.40	4.53	0.08	2.33	0.22	0.63	0.02	0.05	0.00	2.36	0.09
Average Whole Rock	2.87	0.15	0.89	0.07	15.60	0.27	71.63	0.61	3.91	0.13	2.43	0.34	0.56	0.03	0.04	0.01	1.83	0.13
Average Clay Fraction	1.56	0.03	1.53	0.02	19.48	0.03	65.61	0.04	5.61	0.01	2.15	0.01	0.75	0.00	0.06	0.00	3.28	0.01
K-S D value	0.4057		0.2375		0.2396		0.3708		0.3396		0.2271		0.2042		0.2583		0.6271	
probability	0.000		0.001		0.001		0.000		0.000		0.001		0.005		0.000		0.000	
Mann-Whitney U																		
Z-score	6.1178		− 4.38912		− 4.55839		5.97147		− 5.55985		3.541		− 2.6196		− 4.23178		− 10.74	
p value	0.00		0.00		0.00		0.00		0.00		0.0004		0.0088		0.00		0.00	
significant at	< 0.05		< 0.05		< 0.05		< 0.05		< 0.05		< 0.05		< 0.05		< 0.05		< 0.05	

No difference; significant

Note: All values for neither P_2O_5 and SO_3 are 0.00.

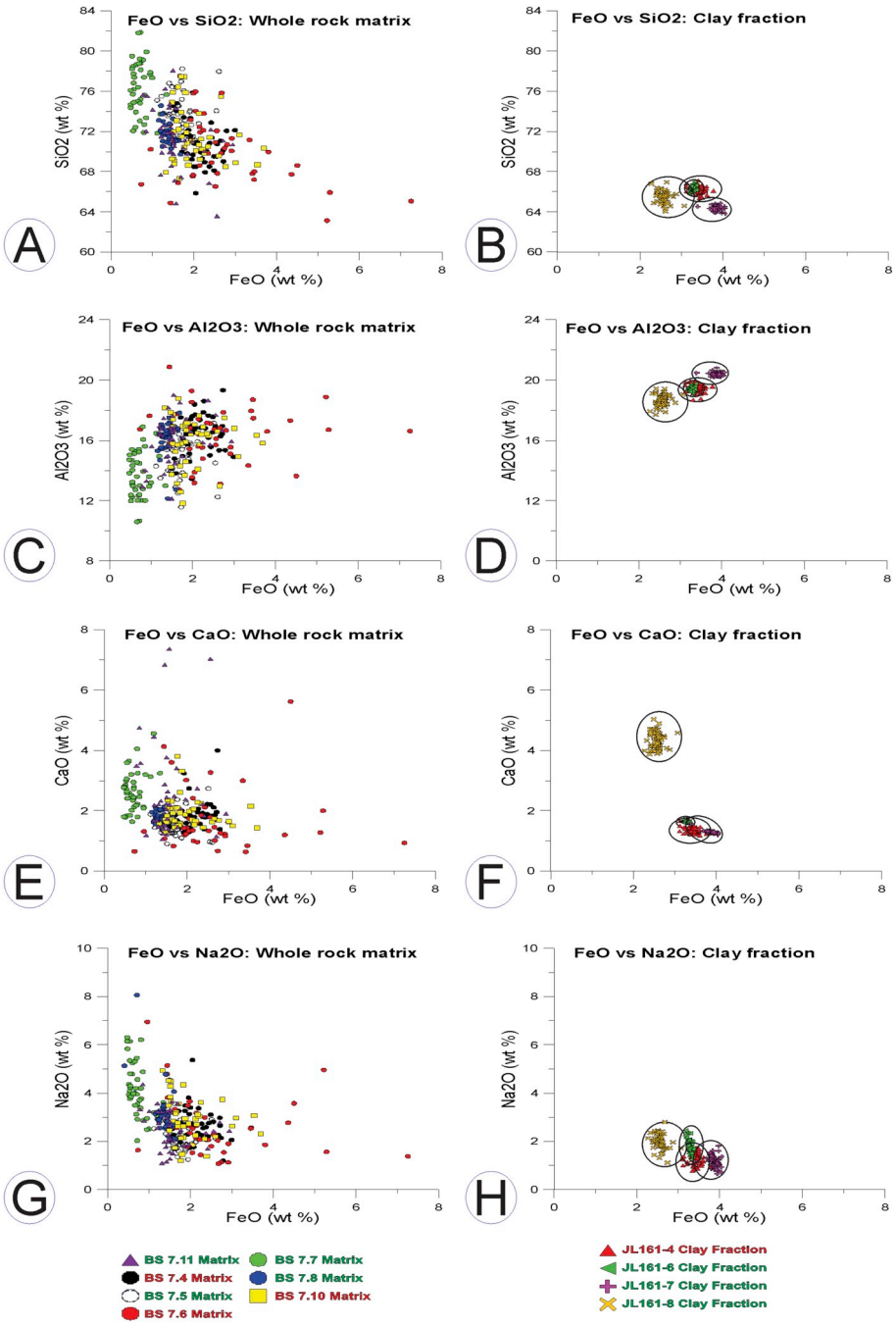

Fig. 8. Bivariate plots of XRF mean elemental values in percent obtained from whole rock (in thin section) and clay-fraction analyses of greenish-gray and grayish-red siltstones. Whole rock and clay fractions are designated by the key, each symbol represents an independent analysis (see text for details). (A) Whole-rock analyses of FeO vs SiO_2. (B) Clay-fraction analyses of FeO vs SiO_2. (C) Whole-rock analyses of FeOvs Al_2O_3. (D) Clay-fraction analyses of FeO vs Al_2O_3. (E) Whole-rock analyses of FeO vs CaO. (F) Clay-fraction analyses of FeO vs CaO. (G) Whole-rock analyses of FeO vs Na_2O. (H) Clay-fraction analyses of FeO vs Na_2O. (I) Whole-rock analyses of FeO vs K_2O. (J) Clay-fraction analyses of FeO vs K_2O. (K) Whole-rock analyses of FeO vs TiO_2. (L) Clay-fraction analyses of FeO vs TiO_2. (M) Whole-rock analyses of FeO vs MgO. (N) Clay-fraction analyses of FeO vs MgO. (O) Whole-rock analyses of FeO vs MnO. (L) Clay-fraction analyses of FeO vs MnO.

also are very similar (see Supplemental information), with minor variance between color suites.

4.2.2. Clay mineralogy

Both greenish-gray and grayish-red siltstone are of the same clay mineralogical composition. All samples are comprised of chlorite (~14 Å) and illite (~10 Å), which are the same clay spectra as reported elsewhere at the same stratigraphic position in other parts of the basin (Gastaldo et al., 2014; Li et al., 2017; see Supplemental data).

4.2.3. Fe^{2+}/Fe^{3+} Concentrations by Mössbauer spectroscopy

Mössbauer spectroscopy provides quantitative data on concentrations of Fe^{2+} and Fe^{3+} in the Bethulie samples (Table 2). Siltstone samples, regardless of color, have > 40% of total Fe in the oxidized state. The grayish-red (BS 7.6) sample has one third more Fe^{3+} when compared to the olive-gray sample (BS 7.11), and at least 26% of total Fe is in the form of dispersed fine-grained hematite. Here, the presence of hematite is restricted exclusively to the sample of grayish-red siltstone.

4.2.4. Iron oxide morphology

The distribution and morphology of different oxide grains were examined for the grayish-red sample (BS 7.6). Clay mineral species identification is based on semi-quantitative elemental compositions via EDS, which is considered to be indicative only of the mineral composition, but cannot be regarded as unequivocal evidence for species identification.

Hematite grains, typically as fine reticulations, primarily occur as coatings on clay minerals. The size of hematite coatings is highly variable, ranging from ~5 μm to as large as ~100 μm, although sizes < 20 μm are most common. Hematite is found most often as coatings on illite and chlorite (Fig. 9), and the former is identified by

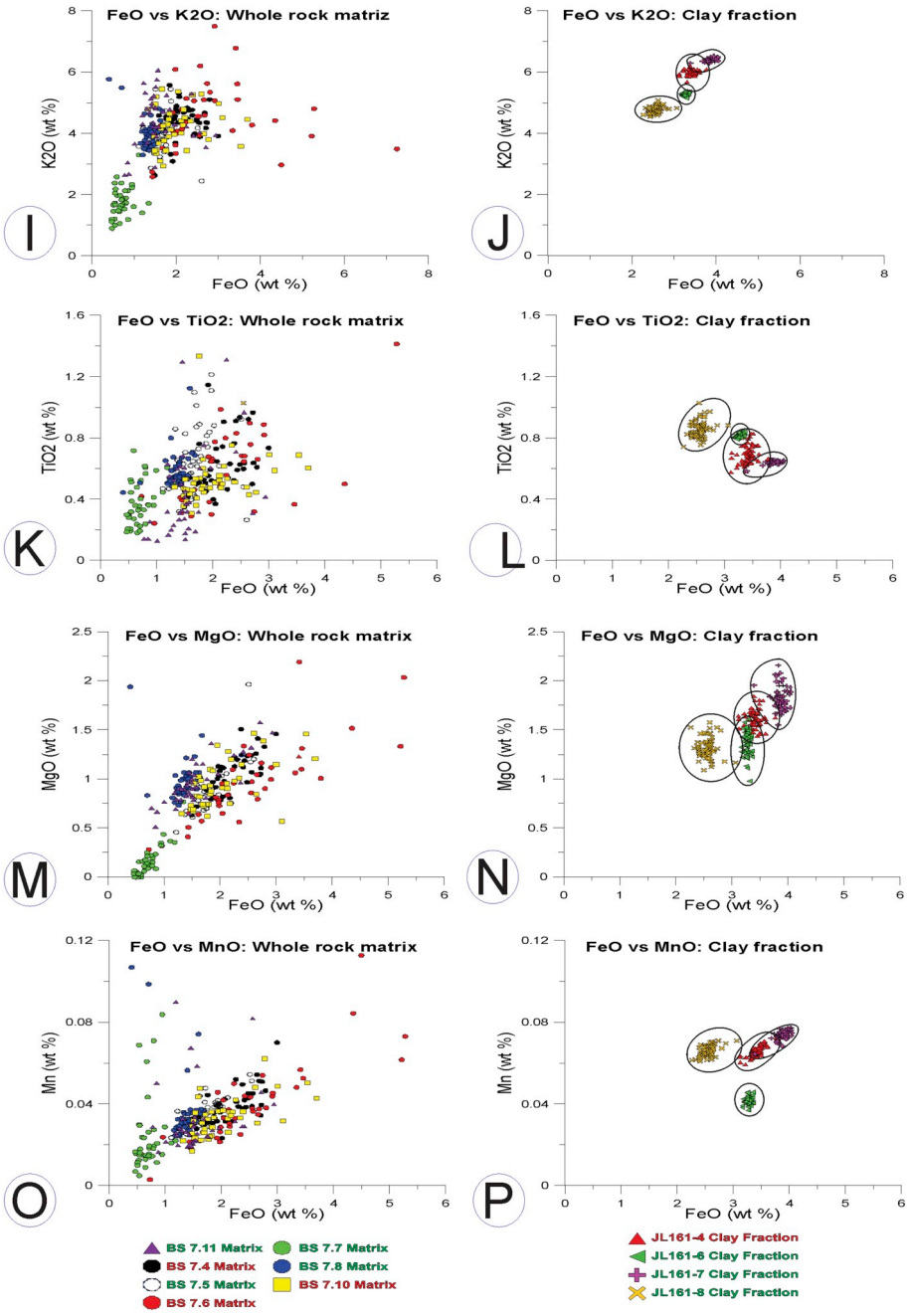

Fig. 8. (*continued*)

the concentration of K in the sample (Table 4) and may contain a significant amount of Fe. Hence, iron in these clay structures likely serves as a source for hematite formation which is suggested by the mineral's reticulated pattern. In addition to hematite, other minerals may contribute to siltstone color including magnetite, rutile, titanite, and ilmenite, all of which are strongly colored and occur in the grayish-red siltstone.

4.2.5. Total organic carbon (TOC)

The mean TOC value of all siltstones in Smith and Botha-Brink's (2014) Facies C is low, 0.29% (Table 3). There is a difference, however, when different colored samples are compared. The mean value of greenish-gray TOC value is lower (0.29%) than those when compared with that of the grayish-red (0.50%) samples. In all samples, except the greenish- and grayish-red JL161-8, TOC:TON (total organic nitrogen) values are < 10, and the average value of these samples is 6.

4.3. Rock magnetic properties

Curves of the acquisition of isothermal remanent magnetization (IRM) for all siltstone samples, regardless of their color, are all concave downward and exhibit a rapid increase in IRM to saturation or near saturation below about 1.0 T (Fig. 10). Backfield DC demagnetization curves yield coercivity of remanence (Hcr) values that are all < 300 mT. Hysteresis measurements show a variable range of response, with coercivities ranging from ~4 to ~13 mT and squareness ratios (Mr/Ms) are highly variable but all below 0.10 (Fig. 11). Response of the bulk susceptibility of siltstone samples as a function of heating and subsequent cooling (Fig. 12) is somewhat uniform, in that all samples demonstrate some degree of irreversible behavior, typically with increases in bulk susceptibility upon cooling to room temperature that range from about 5% to > 25%. To varying degrees, all samples from both greenish-gray and reddish-gray siltstone yield heating/cooling curves

Table 2
Results from Mössbauer spectrography of two Bethulie siltstones demonstrating the quantitative share of Fe^{+2} and Fe^{+3} in each sample, and the percentage of Fe^{+3} as fine grained hematite. Total Fe content of greenish-gray samples is < 1.5%; total Fe content of reddish-gray samples is < 2.5% (see Table 1).

Sample number	Color	Total Fe^{2+} %	Total Fe^{3+} %	Fe^{3+} in octahedral site %	Fe + 3 as fine-grained hematite %	Hematite concentration wt%
B.S.7.6	Reddish-gray (5YR 4/1)	38.36	61.65	36.1	25.55	–
B.S.7.11	Greenish-gray (10Y 6/2)	59.21	40.8	40.8	0	0

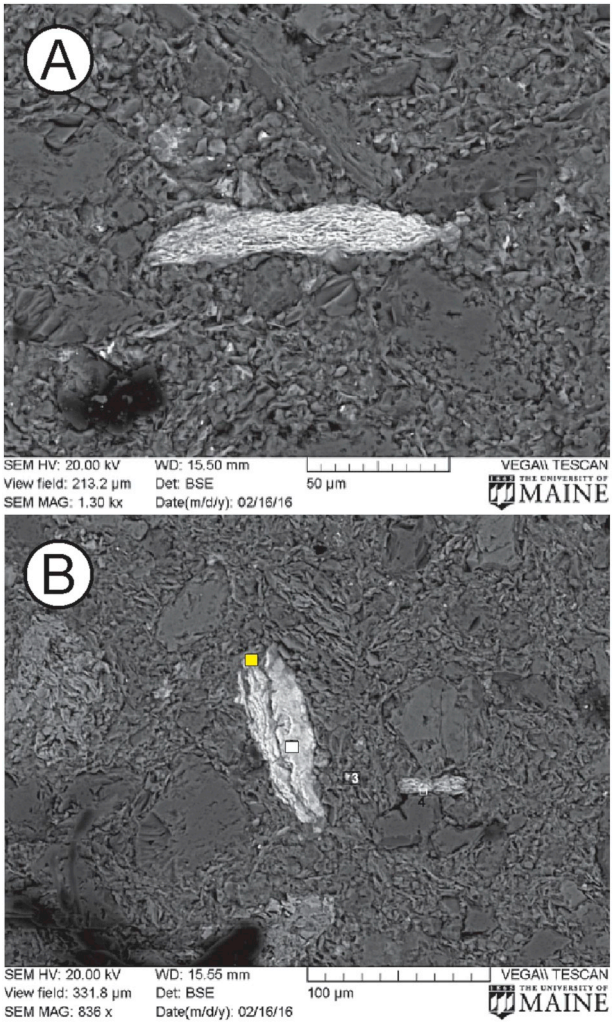

Fig. 9. SEM images of hematite morphologies found on BS 7.6. (A) Hematite coating on clay mineral showing near complete coverage. (B) Reticulate hematite coating on Illite grain; EDS data confirming iron oxide and clay composition obtained from points on clay labeled 1 (white square) and 2 (yellow square), respectively. Scale in µm as shown. (For interpretation of the references to color in this figure legend, the reader is referred to the web version of this article.)

that indicate the presence of a magnetic phase with Curie temperature of about 580 °C, which we interpret to be magnetite. Those samples that show a slight decrease in bulk susceptibility slightly above about 300° to 350 °C in the heating curve (e.g., samples BS7.4, JL161-7, JL161-8, BS7.6, BS 7.5) and the absence of this phenomenon in the cooling curve is interpreted to have a minor concentration of a cation-deficient cubic phase (maghemite). When viewed in a stratigraphic context, there is a distinct similarity between the lowest two samples (JL161-4 and BS7.8) and the uppermost two samples (BS7.7 and BS7.9), as all of these samples are characterized by very low bulk susceptibilities ($< 10 \times 10^{-6}$ SI; mass normalized $< 5 \times 10^{-9}$ m^3/kg). However, all samples in the middle of the sampled section (JL161-5, JL161-6, BS7.4, JL 161-7, JL 161-8, BS7.6, and BS7.5) have susceptibilities that are at least a factor of two higher than the lowest and uppermost samples. In addition, these middle samples all show the presence of minor amounts of maghemite and, in some cases, a slight Hopkinson peak, indicating the presence of coarse magnetite.

Table 3
Total Organic Carbon (TOC) and Total Organic Nitrogen (TON), and TOC:TON of Bethulie greenish-gray and reddish-gray siltstone from Smith and Botha-Brink's (2014) Facies C interval.

	Color	TOC	TON	TOC:TON
JL161-8	Reddish & greenish-gray	0.72	0.04	18
JL161-7	Dark greenish-gray	0.24	0.09	3
JL161-6	Greenish-gray	0.24	0.09	3
JL161-5	Grayish-red	0.38	0.06	6
JL161-4	Mottled greenish/reddish gray	0.41	0.06	7
JL161-3	Greenish-gray	0.25	0.07	4
JL161-2	Greenish-gray	0.37	0.07	5
JL161-1	Greenish-gray	0.37	0.05	7
Average		0.37	0.07	6
Average	Reddish-gray	0.50	0.05	9
	Greenish-gray	0.29	0.07	4
C:N ratio		6		

5. Discussion

The model for the terrestrial response to the end-Permian extinction event revolves primarily around turnover in the vertebrate-fossil record of the Karoo Basin (Ward et al., 2005; Smith and Botha-Brink, 2014; Benton and Newell, 2014; Roopnarine and Angielczyk, 2015; Rubidge et al., 2016). The replacement of the *Daptocephalus* AZ (Viglietti et al., 2016) by the *Lystrosaurus* AZ is reported to occur at the top of a 3–5 m thick interlaminated succession of siltstone, best exemplified in outcrop on the Bethel Farm and designated as Facies C by Smith and Botha-Brink (2014). Smith and Ward (2001) interpreted this lithofacies to represent a response to dramatic climate change, and the interval is reported to be a mappable unit (Smith and Botha-Brink, 2014) that can be correlated across the basin (Ward et al., 2005) and into Antarctica (Retallack et al., 2003). Facies C has been inferred to have been deposited in response to the denudation of vegetation and consequent loss of vertebrate biodiversity over a short < 50 ka time frame (e.g., Smith and Botha-Brink, 2014). Evidence for abrupt and severe drought (Smith and Ward, 2001) as a consequence of climate change is reported to reside in Facies C, interpreted to represent playa-lake deposition (Retallack et al., 2003; Smith and Botha, 2005; Smith and Botha-Brink, 2014). The interpretation that the facies is unique continues to be applied to the Karoo record (Botha-Brink et al., 2014; Viglietti et al., 2016) despite empirical evidence that the facies is spatially and temporally discontinuous on the Bethel Farm, considered to be the type locality at which the boundary is exposed, and elsewhere (Gastaldo et al., 2009; Neveling et al., 2016a, 2016b). This fact has been acknowledged by Ward et al. (2012).

5.1. A critical review of facies C: Playa Lake lithologic types

Smith and Botha-Brink (2014, p. 103) characterize their interlaminated interval at Bethulie as comprised of siltstone-mudstone

Table 4
Elemental data obtained using EDS on clay minerals coated by hematite and Ti-silicates (School of Earth and Climate Science, University of Maine, Orono).

Sample	Na_2O	MgO	Al_2O_3	SiO_2	K_2O	CaO	TiO_2	FeO	Identification
B.S.7.6	0	4.35	19.43	35.05	1.82	0.42	0.26	38.67	Illite
B.S.7.6	0.95	0.28	1.97	5.07	0.52	0.48	23.65	69.09	FeO (Magnetite)

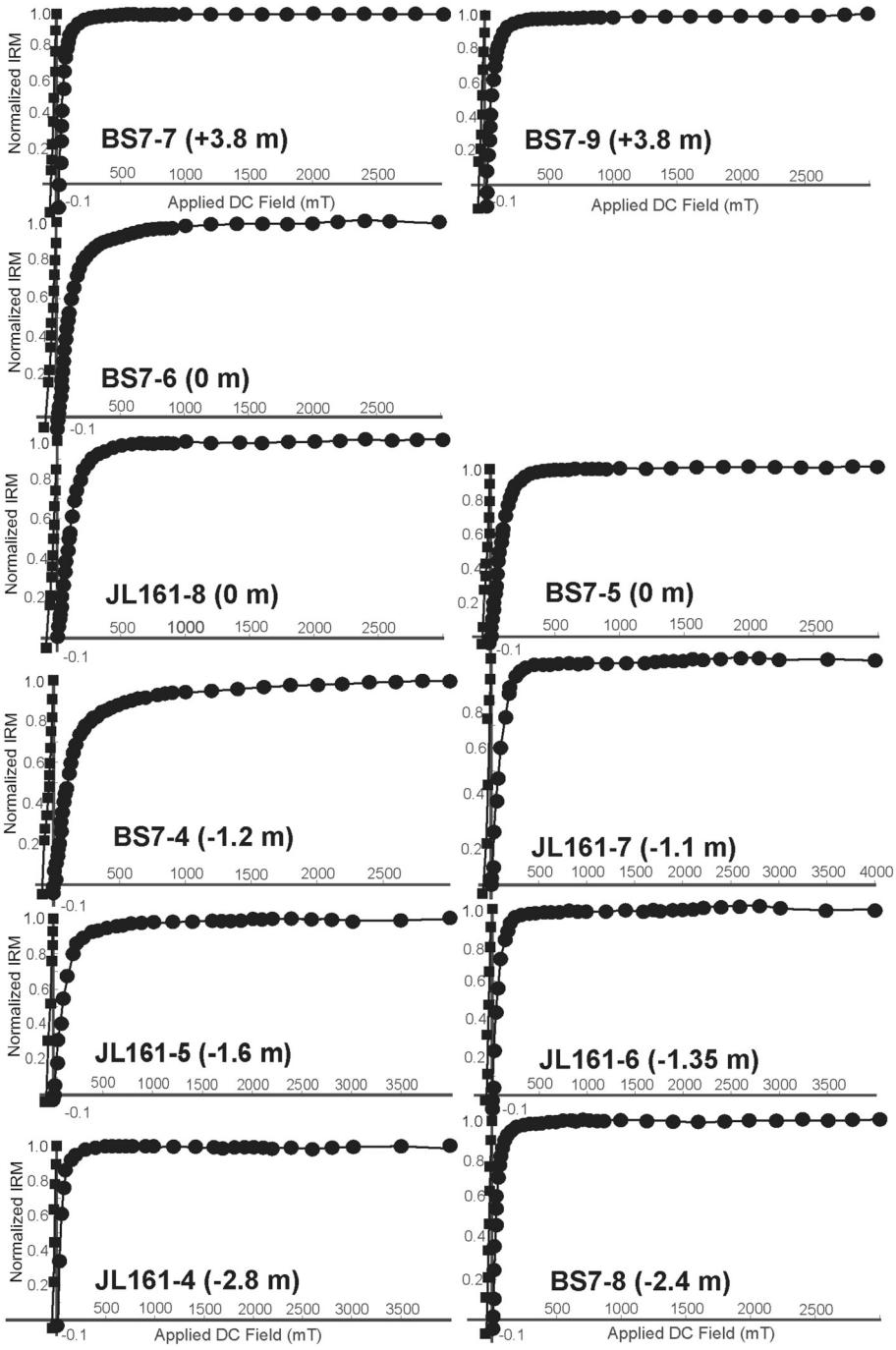

Fig. 10. Results of acquisition of isothermal remanent magnetization (IRM) acquisition experiments to saturation and backfield DC demagnetization for powdered splits of all samples used in this study, arranged in stratigraphic order from bottom to top (0 m = inferred biozone boundary interval). Each specimen was prepared in #04 size gel cap for measurements. Values for saturation IRM (SIRM), anhysteretic remanent magnetization (ARM, acquired in a biasing DC field of 0.1 mT and a peak alternating field of 100 mT), and bulk susceptibility (MS) are indicated for each sample.

(?claystone) couplets that fine upwards, each attaining thicknesses of 1–3 cm. Sandy siltstone is reported to be grayish in color overlain by dark reddish-brown mudstone, and these couplets purportedly can be traced laterally for at least 20 m. Trenching and characterization of the rocks in this specific interval reveal a different set of features than those reported. At this locality (S30.41838°, E026.26785° WGS 84) we find no evidence for interbedded fining up successions on the reported scale. Rather, fining-up successions of greenish-gray to grayish-red siltstone occur as beds on the decimeter scale, and this feature is lost in laterally equivalent beds < 250 m to the southeast, where mottled and greenish-gray siltstone become massive (Figs. 3, 6). Centimeter-scale beds, though, are prominent in laterally equivalent rocks to the northwest on the Heldenmoed Farm (Fig. 6; Gastaldo et al., 2009 and their Supplemental data; S30.41672°, E26.28458° WGS 84).

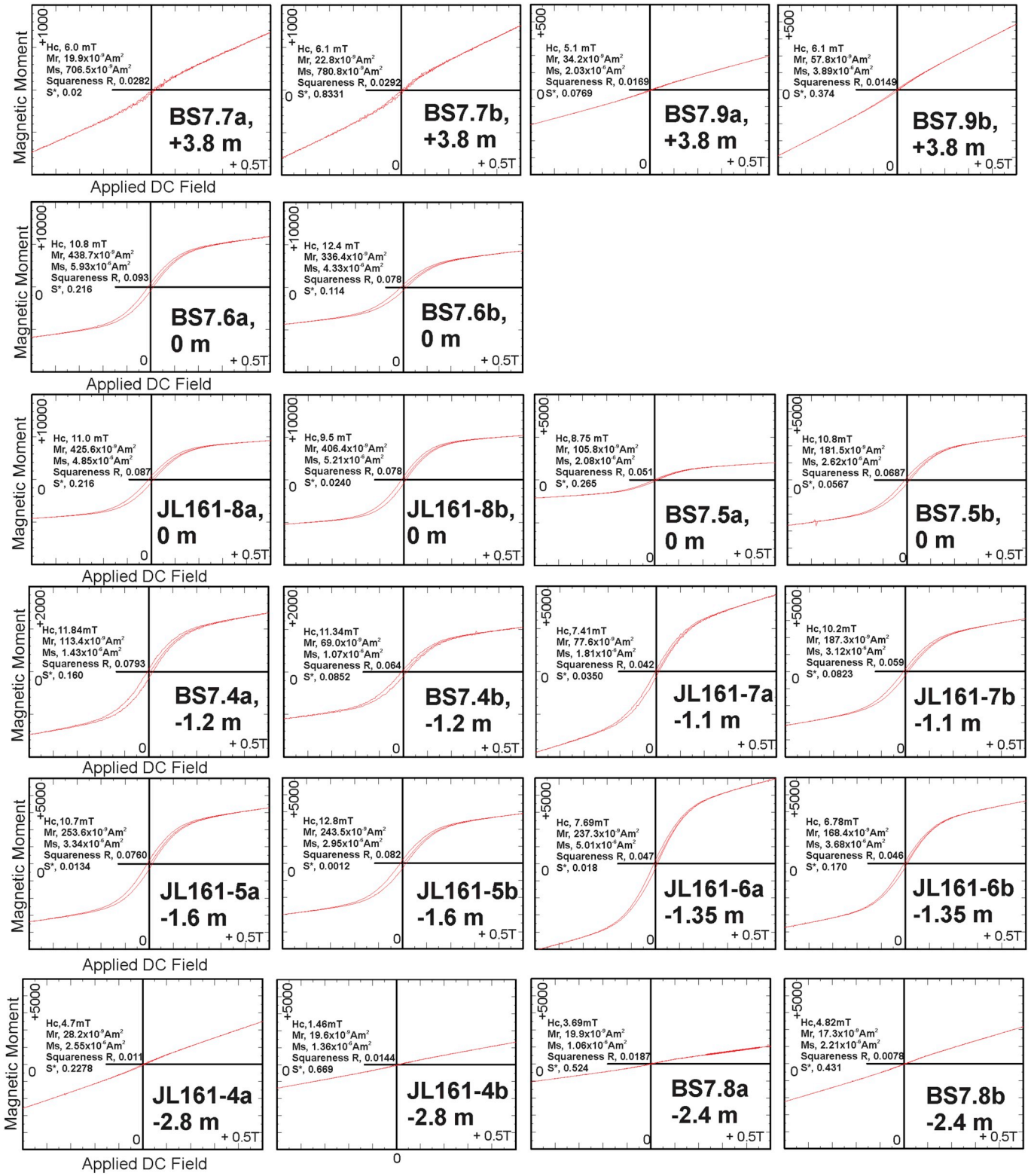

Fig. 11. Magnetic hysteresis curves and related magnetic hysteresis parameters for all samples used in this study, arranged in stratigraphic order from bottom to top (0 m = inferred biozone boundary interval). All curves are obtained with a maximum DC field of (+/−) 500 mT (0.5 T). Note that magnetic moments given on the Y axes are in memu, and have NOT been converted to SI units; the actual values of saturation magnetization (Ms) and saturation remanence (Mr) are in SI units. Hc, coercivity.

Smith and Botha-Brink (2014, p. 105) find no visible evidence of bioturbation, pedogenesis, or desiccation features including authigenic breccias, the latter of which is a criterion used by other workers to identify Permian playa-lake deposits (Hiete et al., 2006; Schneider et al., 2006; Konrád et al., 2010). We, too, find no visible evidence of bioturbation in the Bethel Farm succession (Fig. 2), although burrowing and homogenization are features observed in thin section (Fig. 5C–F). Yet, bioturbation is a visible surficial feature on laterally equivalent, cm-scale beds on the Heldenmoed Farm (Fig. 7B). And, one character originally used by Smith and Ward (2001) to identify this interval is the

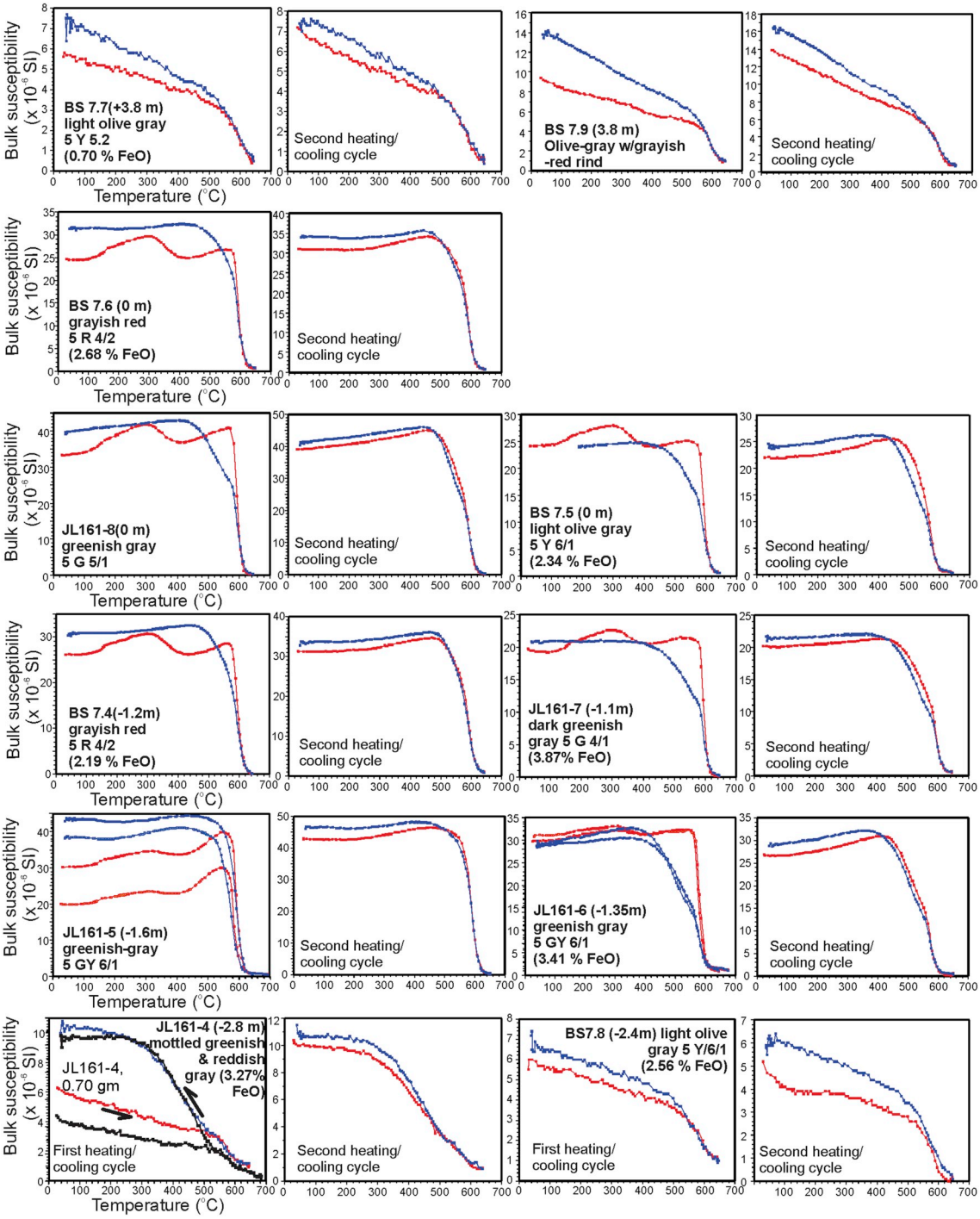

Fig. 12. Plots showing the response of the bulk magnetic susceptibility of powders of all samples used in this study, arranged in stratigraphic order from bottom to top (0 m = inferred biozone boundary interval), as a function of heating and cooling in an inert (argon gas) atmosphere. Arrows indicate the heating (forward) and cooling (backward) curves. All curves are irreversible, with an increase in bulk susceptibility upon cooling. The behavior by some samples showing a decrease in susceptibility over the temperature interval of about 300˚ to 350 ˚C is interpreted to record the conversion of maghemite to hematite. All heating curves reveal the presence of a magnetic phase with a Curie temperature of about 580 ˚C, which is interpreted to be low-titanium magnetite. For all samples, duplicate heating/cooling runs were conducted to evaluate the thermal stability of the assemblage of magnetic phases after the initial heating/cooling experiment. For samples JL161-4, JL161-5, and JL161-6, we show two sets of initial heating/cooling curves.

presence of vertical or inclined *Katbergia* (Gastaldo and Rolerson, 2008) burrows, the only evidence for life in their dead zone. *Katbergia* burrows are found both in the interval exposed on the Heldenmoed Farm and the one documented by Gastaldo et al. (2009) on the Bethel Farm that is ~8 m stratigraphically higher in the section (Neveling et al., 2016a). Although the First Appearance Datum of this burrow was thought to occur in Facies C, it is now known from early Changshingian rocks in the Lootsberg Pass area (Neveling et al., 2016a; Gastaldo et al., 2017). With regard to the report of an absence of pedogenic activity (Smith and Botha-Brink, 2014), we, too, find no physical evidence in the trenched interval for pedogenesis. But, Gastaldo et al. (2009, Supplemental data; Neveling et al., 2016a) illustrate a pedogenically altered silty sandstone with vertical roots directly beneath the interlaminated interval on the Heldenmoed Farm, where the interlaminated interval is only 2.5 m in thickness (Fig. 6).

The Bethulie succession can be compared and contrasted with playa

lake deposits of Permian age that are well known from South America (Zhang et al., 1998) and Europe (e.g., Turner and Smith, 1997; Gaupp et al., 2000; Reinhardt and Ricken, 2000; Hiete et al., 2006; Schneider et al., 2006; Lopez et al., 2008; Brookfield, 2008; Konrád et al., 2010), where such deposits formed in closed basins. In many cases, lithologic criteria, including the presence or evidence of evaporite deposits (Arche, 2008), are used in conjunction with geochemical data (see below) to interpret this depositional environment in the stratigraphic record. Lithologic criteria include the presence of laminated siltstone and mudstone, current-rippled cross-laminated, and climbing and wave-laminated very fine grained sandstone. These features are in direct association with gypsiferous beds, lacustrine carbonate deposits (Zhang et al., 1998; Schneider et al., 2006; Konrád et al., 2010), or calcretes (Reinhardt and Ricken, 2000). Although there is evidence for cross-laminated sandy siltstone in the trenched interval, there is no evidence for any gypsiferous, dolomitic, or calcareous evaporites. Neither Smith and Botha-Brink (2014) report, nor do we find, any evidence for gypsum and/or halite pseudomorphs or dessication features, all characters implicit of evaporitic conditions (Hiete et al., 2006; Schneider et al., 2006; Lopez et al., 2008). Retallack et al. (2003, their Fig. 3) illustrate a thin section of the "boundary" interval at Carlton Heights where acicular crystals are interpreted as a silica-replaced, probably gypsum rosette, but we find no evidence in our thin sections for similar features at Bethel. In addition, although there may be an algal wrinkle preserved in the interlaminated unit in laterally equivalent beds on the Heldenmoed Farm (Gastaldo et al., 2009), we find no evidence of stromatolitic or fenestral structures reported from playa-lake deposits (Zhang et al., 1998; Konrád et al., 2010).

5.2. A critical review of facies C: Playa Lake geochemistry

Playa lake deposits are characterized geochemically by the presence of evaporite minerals, ranging from dolomites and carbonates, to halite, tronahalite, and gypsum, and may contain an array of authigenic clay minerals (Calvo et al., 1999). As Smykatz-Kloss and Roy (2010) note, the physical and chemical conditions affecting a playa-lake setting ultimately will determine the fate of these minerals. And, as Hiete et al. (2006) demonstrate, geochemical proxies are related to the grain size of the sample assessed, necessitating the elimination of grain fractions (i.e., sand and silt) that bias results towards high aluminosilicate values. Although we have not encountered any cm-scale or dm-scale bed of evaporite origin in either the trenched or laterally equivalent intervals (Fig. 6), the geochemistry and clay mineralogy of the greenish-gray and grayish-red siltstone in this interval, shown to be indistinguishable in major-and-minor element values and clay species, should retain some elemental signature of evaporative conditions provided such conditions had existed.

A number of studies on Recent playa lakes focus on brine geochemistry (e.g., Bowen and Benison, 2009), with few reporting on the chemical nature of clastic lake sediments, other than evaporites, found therein (e.g., Draper and Jensen, 1994; Gill et al., 2002; Shütt, 2004). Also, whereas a limited number of Permian deposits are characterized geochemically, these authors note post-burial, diagenetic elemental enrichment and depletion of elements (e.g., Varga et al., 2005), making comparison with the Bethel interval difficult. Draper and Jensen (1994) may provide one of the more extensive characterizations of clastic sediments from Lake Frome in Australia, where they analyzed 94 samples for Cu, Pb, Zn, Mn, V, Fe, SO_4, of which 10 samples were assessed for major elements. And, although Gill et al. (2002) evaluated three different suites of saline crust in Owens Lake, California, which they deemed suitable for entrainment by wind and transport, and Shütt (2004) characterized sediments associated with a full spectrum of evaporite minerals in the Ebro Basin, Spain, the absence of deposits of carbonate and/or gypsum at Bethulie makes comparison with these sets of geochemical data meaningless. Hence, a comparison is made with Draper and Jensen's (1994) Lake Frome geochemical data because their major element analyses are corrected to zero water soluble NaCl.

Draper and Jensen (1994) report a low percentage of organic carbon in Lake Frome sediments, averaging 0.29%. TOC values in Bethulie siltstone range from 0.24 to 0.72%, averaging 0.37%, with higher concentrations found in the grayish-red samples (Table 3). TOC:TON values are < 10, indicating that the organic matter contribution originated from an algal source (Brown et al., 1998). The influx of terrigenous organic matter near the top of the interval is signaled by a change in TOC:TON ratio in sample JL161-8 (C:N = 18; mottled greenish- and reddish-gray).

Weight percentages of three major elements in the Bethulie siltstones are significantly higher than to those reported from Lake Frome, whereas the remaining elemental concentrations are significantly lower. Specifically, SiO_2 in Bethulie siltstones average 69% when compared with a value of 47% in the Australian site, with a similar disparity in Al_2O_3 (17.01% vs 12.9%) and K_2O (4.53% vs 2.14%). In contrast, weight percentages of total Fe (2.36% vs 4.46%), CaO (2.33% vs 6.47%), MgO (1.12% vs 2.82%), and SO_2 (undetected 0% vs 5.52%) all are lower in Bethulie samples. A prominent difference is noted when comparing the proportion of minor elements in the Australian versus Bethulie site.

Values for Cu (27.83 ppm vs 3.5–12 ppmw), Pb (12.29 ppm vs 10–13 ppmw), Zn (73.11 ppm vs 15–30 ppmv), and V (150.08 ppm vs 20–55 ppmv) all are significantly higher in the sediments of the Recent playa lake than in Bethulie siltstone (see Supplemental data). Kistler and Helvaci (1994) note that such deposits also have a higher proportion of borates, with elevated Boron levels. Boron values in Bethulie samples are low, ranging from 65 to 70 ppmv, as are those for lithium (12–32 ppmv), both of which are low for a playa-lake deposit. Other elemental concentrations are reported from Permian playa deposits (e.g., Hiete et al., 2006; Konrád et al., 2010) which also differ from the Bethulie samples.

Authigenic clay minerals often are a component of evaporite successions in ephemeral continental lakes (Calvo et al., 1999). These include, but are not restricted to, Mg-rich smectites, kerolite, sepiolite, and palygorskite. We find no evidence of any one or more of these typical authigenic clay species in our samples. Rather, the presence only of illite and chlorite in the Bethulie interval parallels the same clay mineralogical assemblage found in Inceptisols of the *Daptocephalus* AZ at Wapadsberg Pass (Gastaldo et al., 2014) and in both greenish-gray and grayish-red siltstone at Old Lootsberg Pass (Li et al., 2017).

5.2.1. An explanation for grayish-red siltstone coloration

One feature deemed characteristic of aridification processes, and used by Smith and Botha-Brink (2014) and others to infer catastrophic climate change in the upper *Daptocephalus* AZ, is the appearance of grayish-red siltstone. Color modification from greenish-gray to reddish-gray is envisioned to be a consequence of wind-blown (loessic) red silt grains that were deposited in beds of uniform texture, and characteristic of the overlying massive maroon-siltstone facies (Facies D; Smith and Botha-Brink, 2014). Smith and Botha-Brink (2014, p. 105) express confidence that the reddening is a primary feature and a function of settled iron-oxide particles incorporated into overbank (floodplain) sediment via pedogenesis. Hence, although deposition of these fine clastic deposits is not attributed solely to a loessic origin, their color modification is considered a function of eolian activity, imparting a red color.

Our data indicate that the main difference between the greenish-gray and grayish-red siltstone at Bethulie, and elsewhere in the Karoo Basin (Li et al., 2017), is the presence or absence of a low amount of hematite (Table 2). Mössbauer spectroscopy indicates that there is a higher percentage in total Fe^{+2} in greenish-gray siltstone than in grayish-red siltstone, and vice versa for Fe^{+3}. There is essentially no difference in the percentage of Fe^{+3} in octahedral sites. The difference between the two siltstone types is in the very low percentage (< 1 wt %) of fine-grained hematite in grayish-red samples, one of several

minerals present that impart a grayish-red color to this siltstone type (Li et al., 2017). SEM analyses of the clay fraction (Fig. 9) demonstrate that hematite does not occur as isolated detrital grains (e.g., relatively coarse specularite) or other forms of particles (e.g., as products of the oxidation of ferromagnesian silicates) independent of clay minerals. The rock-magnetic properties obtained for these rocks are, at least, consistent with these observations. Because of the substantial difference in grain size between authigenic hematite as mineral coatings and detrital, silt-sized or coarser hematite grains (specularite), many workers have investigated the control that particle size, among other parameters, has on the rock magnetic properties of hematite (e.g., Banerjee, 1971; Dunlop, 1971; Ozdemir and Dunlop, 2014). The fact that IRM acquisition curves show a progressive increase in IRM intensity well beyond 1.0 T is consistent with the abundance of fine, submicron authigenic hematite, which is characterized by high coercivities. Although we have not performed progressive thermal demagnetization experiments on these materials, which would reveal laboratory unblocking temperature spectra, we plan to conduct such experiments in the future. We predict that the abundance of fine, pigmentary hematite will be documented as a spectrum of relatively low laboratory unblocking temperatures, well below the Neel temperature of pure hematite (about 680̊ C). Rather, hematite occurs as a fine coating on clay minerals, and is an early diagenetic process attributed at Old Lootsberg Pass to water-chemistry fluxes in standing bodies of water (Li et al., 2017). The reddish color in other Permian-aged successions of a playa lake origin is attributed to a high hematite/FeO ratio which, in the case of the Boda Siltstone, SW Hungary, is about 7 (Konrád et al., 2010). The hematite/FeO ratio in the Bethulie samples is 0.3. Hence, we find no evidence to support siltstone-color alteration from greenish-gray to grayish-red through the incorporation of wind-blown hematite and suspension of pedogenic processes in playa-lake deposits as suggested by Smith and Botha-Brink (2014). We also note that the hematite/FeO ratio does not approach that reported in Permian playa deposits where the oxide ranges from 6 to 10% (Konrád et al., 2010). We interpret the mottled greenish- and grayish-red siltstones to be a function of fluctuations in paleowater table as reported elsewhere (Kraus and Hasiotis, 2006; Lopez et al., 2008; Li et al., 2017).

5.3. Rock magnetic properties and magnetic polarity stratigraphy

Smith and Botha-Brink (2014, p. 105) report that Facies C at Bethulie coincides with a geomagnetic field polarity reversal, as purportedly reported by other workers (Steiner et al., 2003; Ward et al., 2005). We note here that Steiner et al. (2003) do not provide any magnetic polarity stratigraphic information for rocks at Bethulie or elsewhere. Rather, Schwindt et al. (2003) provide these data for the Carlton Heights section (Pace et al., 2009). However, none of these contributions adequately demonstrate the preservation of a reverse polarity remanence in these rocks. This polarity reversal, from reverse to normal polarity, some 200 ka prior to the end of the Permian (Szurlies, 2013), is a critical geologic datum that seemingly has been correlated with data from marine Permo–Triassic boundary sections in China in which a high-precision geochronologic framework has been developed (Burgess et al., 2014; Szurlies, 2013; Hounslow and Balabanov, 2016). The polarity reversal also has been correlated with a reverse-to-normal polarity interval that has been interpreted to exist in some other sections in the Karoo Basin, yet without adequate documentation. We have conducted extensive paleomagnetic sampling of the Bethulie section (over 50 stratigraphic intervals as independent sampling sites), as well as other key sections in the Karoo Basin (Old Lootsberg Pass, Gastaldo et al., 2015; Kommandodrif Dam, Neveling et al., 2016a) in an attempt to develop a robust magnetic polarity stratigraphy for these rocks. Although this contribution does not report any of the paleomagnetic data from the Bethulie section, we do offer an important caution regarding the interpretation of any data from any Permian/Triassic boundary section in the Karoo Basin. The

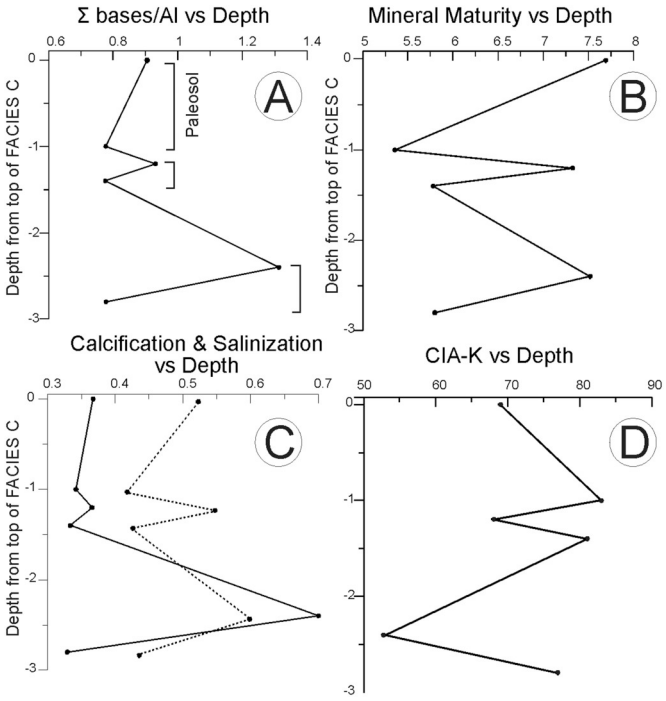

Fig. 13. Selected coarse geochemical proxy profile of Facies C in which a minimum of 3 paleosols are interpreted in the siltstone succession. (A) Σ of base loss ([Na + Ca + K + Mg]/Ti) versus depth from the top of Facies C showing three intervals in which there is a decrease in the weathering proxy. (B) Mineral Maturity (Si/Al) versus depth. (C) Calcification ([Ca + Mg]/Al; solid line) and Salinization ([K + Na]/Al; dashed line) versus depth. (D) Plot of siltstone profile of CIA-K (Chemical Index of Alteration minus potassium); note values calculated for all samples except 161-7 and 161-4 are based on whole-rock analyses.

paleomagnetic record of these rocks is complicated by the fact that there is a potential for widespread, pervasive partial-to-complete remagnetization of basin successions as a result of the emplacement of the very large volume of mafic intrusions of the ca. 183 Ma Karoo Large Igneous Province. Our studies in the Bethulie area involve the acquisition of multiple (i.e., 7–10 +) independent samples at every level collected, as well as detailed contact tests with Karoo dikes, the typical thickesses of which are < 1.5 m (Neveling et al., 2016a, 2016b). Results from these investigations are in preparation.

The rock magnetic data from representative samples of greenish-gray and grayish-red siltstone show no clear distinction in magnetic mineralogy between the two siltstone types. In fact, the data are interpreted to indicate considerable similarity between them. The most noticeable observation in the rock magnetic data is the enhanced, by at least a factor of two, bulk magnetic susceptibility of all samples, regardless of their color, collected in the two-meter interval below, as well as just at, the inferred biozone boundary interval (Fig. 12). Curves of the acquisition of an IRM and backfield demagnetization of saturation or near-saturation IRM show that all samples analyzed contain an abundance of a relatively low coercivity cubic phase. A reasonable interpretation of these data is that a combination of magnetite and maghemite, in varying abundance, is the source of this behavior. The fact that there is an increase in IRM intensity in fields higher than about 300 mT indicates the presence of some hematite. Many samples of greenish-gray, as well as grayish-red/reddish-brown siltstone show a sharp rise in IRM intensity well below 300 mT, indicating an abundance of low coercivity cubic phases (e.g., magnetite and/or maghemite). Subsequently, there is a progressive and significant increase in IRM intensity over a range of peak fields between about 1.0 T and close to 3.0 T. These data indicate the presence of hematite, although below detection limits at Mössbauer levels in the former. The overall geometry of all hysteresis curves from samples collected within two meters below and

just at the inferred biozone-boundary interval further demonstrates the abundance of relatively low coercivity cubic phases. The squareness ratio for each of the samples indicates the relatively coarse grained nature of the cubic phases. Bulk susceptibility vs. temperature experiments are perhaps the most informative of the data sets, as they reveal the clear distinction between samples collected within 2 m of the biozone-boundary interval and those farther below or above the interval. Notably, samples collected in this interval have higher susceptibilities and consistently display evidence for minor amounts of maghemite. The available geochemical data indicate that this difference is not obviously correlated with total FeO concentration (Fig. 12). The distinct presence of maghemite in this interval of sedimentary rocks with higher bulk susceptibilities prompts the question as to its origin in the context of possible environmental changes during deposition, and this continues to be the subject of further investigation.

6. If not, then what

Gastaldo et al. (2009) interpreted the depositional environment of the interlaminated facies interpreted by Smith and Ward (2001) as the "event bed," and used by others (Retallack et al., 2003; Ward et al., 2005; Smith and Botha, 2005) to mark the PTB, as an abandoned channel-fill succession. Primary sedimentary structures exposed on the Heldenmoed Farm, which include low amplification, asymmetrical, ladder, and interference ripples (Fig. 7), are indicative of a bedload origin and/or modification of the sediment-water interface under shallow-water conditions. The fact that horizontal burrows and possible algal wrinkle structures are preserved on the upper bed contacts of sandy coarse siltstone also are evidence for low flow or quiet water conditions in a fully aquatic setting. The presence of *Katbergia* (Gastaldo and Rolerson, 2008) in the upper part of the interval demonstrates that burrowing occurred when watertable levels lowered sufficiently, exposing saturated sediments that were not dried out to colonization. These are features also documented at Old Lootsberg Pass by Li et al. (2017). And, the fact that this suite of characters occurs at several different stratigraphic horizons in the Bethulie area (Gastaldo et al., 2009; Neveling et al., 2016a, 2016b) indicates that the depositional environment was neither unique nor synchronous; this fact was acknowledged by Ward et al. (2012). Hence, the facies that is spatially and temporally restricted. The lateral equivalent of the channel-fill succession on the Heldenmoed Farm (Figs. 2, 6), identified by Smith and Botha-Brink (2014, their Fig. 5) as their Facies C on the Bethel Farm (Figs. 4, 6) doesn't display the same suite of characters and displays no features that allow it to be characterized as interlaminated.

The lithologic succession that is used to typify the transition from the *Daptocephalus* to the *Lystrosaurus* AZs consists of several fining up beds of up to 40 cm in thickness, of sandy coarse or coarse siltstone (near the base) grading to fine siltstone. There is no evidence of any pattern exhibiting alternating greenish-gray and reddish-gray coloration on a cm-scale basis. The interval is dominated by the former hue (Fig. 4). Small-scale lamination is preserved in the basalmost part, with sediment homogenization being common in all other thin sections (Fig. 5). Some evidence exists for bioturbation, although burrow margins are not prominent. The physical characteristics of Smith and Botha-Brink's (2014) Facies C conform to those of a Protosol (Mack et al., 1993).

The strategy of sampling the trenched interval was to collect competent beds from which thin sections could be made to assess whether or not interlamination was prominent in Facies C. Hence, sampling at Bethulie was at a coarser scale than that undertaken by Li et al. (2017) for an interlaminated interval at Old Lootsberg Pass. Nevertheless, coarse trends of weathering proxies (Sheldon and Tabor, 2009) are interpreted to represent the presence of a minimum of three paleosol profiles in the interval (Fig. 13). There are marked, decreases in values in the Σ base loss/Al, a proxy for the degree to which a soil is leached, with increasing depth (Fig. 13A). The elevated value at 2.4 m depth is the result of high Ca values in that sample (Fig. 13C) which may be a function of calcite cement. Trends in Mineral Maturity (Fig. 13B) and Salinization (Fig. 13C) parallel those of base loss. CIA-K values and trends range from a low of 63 to a maximum of 81 (Fig. 13D) with two maxima, at depths of 1.4 and 2.8 m, originating from the clay fraction. Yet, the value originating from the whole-rock sample at 1.0 m is similar, intimating that the sample fraction has not biased the calculated results. Hence, CIA-K values mimic the coarse trends of interpreted paleosols, with moderate to high values indicative of more intense weathering conditions under warmer and wetter climate states (Nesbitt and Young, 1982). These values are similar to those reported by Gastaldo et al. (2014) for Inceptisols at Wapadsberg Pass. The weathering indices of Bethulie siltstones are additional evidence negating a playa-lake interpretation for Smith and Botha-Brink's (2014) Facies C.

7. Conclusions

We have undertaken a multi-disciplinary examination of a non-unique lithofacies (Gastaldo et al., 2009; Ward et al., 2012; Gastaldo and Neveling, 2012, 2016; Neveling et al., 2016a; Rubidge et al., 2016) used by many other workers (Ward et al., 2005; Smith and Botha, 2005; Botha and Smith, 2006, 2007; Smith and Botha-Brink, 2014; Botha-Brink et al., 2014; Rey et al., 2016; Viglietti et al., 2016) as the key stratigraphic horizon where vertebrate turnover is reported from the *Daptocephalus* (formerly *Dicynodon*; Viglietti et al., 2016) to the *Lystrosaurus* Assemblage Zone, the dynamics of which have been interpreted to mark the end-Permian extinction event on land (Ward et al., 2005; Benton and Newell, 2014; Rubidge et al., 2016). We have characterized the > 3 m interval exposed on the Bethel Farm, Bethulie, Free State, using field relationships, petrographic and geochemical analyses, and rock magnetic properties. From these, we provide data to test the interpretation of the interval as representative of playa-lake deposition as a consequence of aridification.

The short stratigraphic interval terminating the *Daptocephalus* AZ figured by Smith and Botha-Brink (2014, their Fig. 5) on the Bethel farm is reported as an interlaminated succession of 1–3 cm thick siltstone-and-mudstone couplets, with the coarser fraction characterized as a gray color and the overlying fine fraction as reddish-brown in color (Smith and Botha-Brink, 2014, p. 103). The succession is described as having no visible evidence for bioturbation, pedogenesis, or desiccation. Our physical data that originate from this figured locality demonstrate an absence of bedding at the cm-scale, but dm-scale fining up successions. Basal beds contain mm-scale, low-angle cross and parallel lamination on the sub-mm scale. These competent beds are overlain by thick, decimeter-scale homogenized beds in which evidence exists for low-angle lamination and burrows that appear horizontal in thin section. < 360 m to the northwest, however, this succession grades laterally to a short (< 3 m thick) interval in which cm-scale laminated sandstone-and-mudrock successions are exposed. These beds preserve ripples at the contacts between coarse and fine fractions, horizontal burrows, and vertically oriented *Katbergia* burrows, as documented previously by Gastaldo et al. (2009, their Supplemental data). In the opposite direction, within 160 m to the southeast, the succession grades laterally to mottled greenish-gray siltstone and then, 60 m farther, to massive olive gray siltstone, without any evidence of siltstone-mudstone couplets or lamination; again, features previously documented by Gastaldo et al. (2009, their Fig. 3). And, although laminated couplets of fine-grained sediments are one criterion associated with playa or, for that matter, a range of lake deposits (Carroll and Bohacs, 1999; Bohacs et al., 2000), we also find no evidence in outcrop or thin section of any evaporite (gypsum, dolomite, carbonate) in the succession, either in the form of planar beds or pseudomorphs, which is a criterion on which other Permian playa-lake deposits are interpreted (Reinhardt and Ricken, 2000; Hiete et al., 2006; Schneider et al., 2006; Konrád et al., 2010). The physical evidence is such that Facies C of Smith and Botha-Brink (2014) can neither be traced physically over 200 m laterally

along strike at Bethulie, nor are its reported features consistent in outcrop across this distance. The rock magnetic data reveal no appreciable differences in the magnetic mineralogy of greenish-gray and reddish-brown siltstone collected at similar stratigraphic intervals. And, in addition, the geochemical data we report here do not support a depositional environment interpretation of a playa lake for these rocks.

In the absence of calcrete (Reinhardt and Ricken, 2000; Schneider et al., 2006), dolomite (Turner and Smith, 1997; Reinhardt and Ricken, 2000; Konrád et al., 2010), gypsum (e.g., Shütt, 2004), or pyritic (Konrád et al., 2010) beds characteristic of Permian playa lakes, an evaluation of major, minor, and trace elements in Bethulie siltstones might have provided unequivocal evidence in support of such an interpretation. Geochemical data from the Bethulie-siltstone interval reveal that values do not differ from major and minor element geochemical data previously reported from the *Daptocephalus* AZ (Retallack et al., 2003; Coney et al., 2007; Gastaldo et al., 2014). When compared with geochemical data from Recent Lake Frome sediments, corrected to zero water-soluable NaCl, Si, Al, and K weight percentages in Bethulie are significantly higher than values reported, whereas Fe, Mg, Na, and S values are significantly lower. Boron, a common constituent of playa lake sediments (Kistler and Helvaci, 1994), is lower than what might be expected for such deposits. Notably, concentrations of Cu, Pb, Zn, and V are all significantly higher in the Lake Frome sediments than in Bethulie siltstone of any siltstone color. The fact that geochemical data from the Bethulie interval are similar to Inceptisols from Wapadsberg Pass (Gastaldo et al., 2014) and other *Daptocephalus* AZ siltstones (Retallack et al., 2003; Coney et al., 2007), and show no enrichment in elements common in other playa deposits (Draper and Jensen, 1994; Varga et al., 2005), leads us to conclude that there is no elemental evidence to support the interpretation of Smith and Botha-Brink (2014) that their Facies C represents a playa-lake deposit nor that silt in these rocks is of eolian origin. Rather, these data support previous interpretations in other latest Permian localities (Neveling et al., 2016a, 2016b; Gastaldo et al., 2014, 2017; Li et al., 2017) that wetter conditions prevailed during the reported transition from the *Daptocephalus* to *Lystrosaurus* assemblage zones in the Karoo Basin of South Africa.

Acknowledgments

The authors appreciate the hospitality, kindness, and property access shown to them over past decade by Pieter and Ansie Grobbelaar, Caledon River Holiday Farm, Free State. Field assistance by S. Makubalo (Council for Geoscience), and S. Gray, D. Pace, S. Newbury, C.K. Clark, O. Battifarano, and A. Churchill (Colby College) are acknowledged. N. Tabor and M. Meredith, Southern Methodist University, and D. Dyar, Mt. Holyoke College, are thanked for their assistance with clay mineralogy and Mössbauer spectroscopy, respectively, and M. Yates, University of Maine, Orono, for assistance with SEM imaging, and M. Abdulkadir and K. Ables for assistance with the collection of rock magnetic data in the UTD laboratory. Reviews by Spencer Lucas, Jörg Schneider, and Wan Yang are appreciated. Research efforts were supported, in part, by: the Council for Geoscience (South Africa); NSF EAR 0749895, 0934077, 1123570 and 1624302; and a Fulbright Scholar Award from the U.S. Department of State to RAG.

Appendix A. Supplementary data

Supplementary data to this article can be found online at http://dx.doi.org/10.1016/j.earscirev.2017.08.002.

References

Abdala, F., Cisneros, J.C., Smith, R.M.H., 2006. Faunal aggregation in the early Triassic Karoo Basin: earliest evidence of shelter-sharing behavior among Tetrapods? PALAIOS 21, 507–512.

Arche, A., 2008. Some precisions on the use of the term *playa* in the geologic literature. J. Iber. Geol. 34, 5–9.

Banerjee, S.K., 1971. New grain size limits for palaeomagnetic stability in hematite. Nature Phys. Sci. 232, 15–16.

Benton, M.J., Newell, A.J. (Eds.), 2014. Impact of global warming on Permo-Triassic terrestrial ecosystems. Gondwana Res. 25, 1308–1337.

Lake-basin type, source potential, and hydrocarbon character: an integrated-sequence-stratigraphic– geochemical framework. In: Bohacs, K.M., Carroll, A.R., Neal, J.E., Mankiewicz, P.J., Gierlowski-Kordesch, E.H., Kelts, K.R. (Eds.), Lake Basins Through Space and Time: AAPG Studies in Geology. 46. pp. 3–34.

Boonstra, L.D., 1969. The fauna of the *Tapinocephalus* zone (Beaufort beds of the Karoo). Ann. S. Afr. Mus. 56 (73 p.).

Botha, J., Smith, R.M.H., 2006. Rapid vertebrate recuperation in the Karoo Basin of South Africa following the end-Permian extinction. J. Afr. Earth Sci. 45, 502–514. http://dx.doi.org/10.1016/j.jafrearsci.2006.04.006.

Botha, J., Smith, R.M.H., 2007. *Lystrosaurus* species composition across the Permo–Triassic boundary in the Karoo Basin of South Africa. Lethaia 40, 125–137.

Vertebrate paleontology of nooitgedacht 68: a *Lystrosaurus maccaigi*-rich Permo-Triassic boundary locality in South Africa. In: Botha-Brink, J., Huttenlocker, A.K., Modesto, S.P., Kammerer, C.F., Angielczyk, K.D., Fröbisch, J. (Eds.), Early Evolutionary History of the Synapsida, Vertebrate Paleobiology and Paleoanthropology. Springer, Dordrecht, pp. 289–304. http://dx.doi.org/10.1007/978-94-007-6841-3_17.

Botha-Brink, J., Codron, D., Huttenlocker, A.K., Angielczyk, K.D., Ruta, M., 2016. Breeding young as a survival strategy during Earth's greatest mass extinction. Sci Rep 6, 24053. http://dx.doi.org/10.1038/srep24053.

Bowen, B.B., Benison, K.C., 2009. Geochemical characteristics of naturally acid and alkaline saline lakes in southern Western Australia. Appl. Geochem. 24, 268–284.

Brookfield, M.E., 2008. Palaeoenvironments and palaeotectonics of the arid to hyperarid intracontinental latest Permian-late Triassic Solway basin (U.K.). Sediment. Geol. 210, 27–47.

Broom, R., 1906. On the Permian and Triassic faunas of South Africa. Geol. Mag. 3, 29–30 (Decade V).

Brown, S.L., Bierman, P.R., Mehrtens, C.J., Lini, A., 1998. Terrigenous layers in lake cores document fluctuations in New England's Holocene climate. In: GSA Abstracts with Programs. 81. pp. 2523–2524.

Burgess, S.D., Bowring, S., Shen, S., 2014. High-precision timeline for Earth's most severe extinction. PNAS 111, 3316–3321.

Calvo, J.P., Blanc-Valleron, M.M., Rodríguez-Arandía, J.P., Rochy, J.M., Sanz, M.E., 1999. Authigenic clay minerals in continental evaporite environments. Int. Assoc. Sedimentol. Spec. Publ. 27, 129–151.

Carroll, A.R., Bohacs, K.M., 1999. Stratigraphic classification of ancient lakes: Balancing tectonic and climatic controls. Geology 27, 99–102.

Cluver, M.A., Hotton, N., 1981. The genera *Dicynodon* and *Diictodon* and their bearing on the classification of the Dicynodontia. Ann. S. Afr. Mus. 83, 99–146.

Coney, L., Reimold, W.U., Hancox, J., Mader, D., Koeberl, C., McDonald, I., Struck, U., Vajda, V.O.L., Kamo, S.L., 2007. Geochemical and mineralogical investigation of the Permian-Triassic boundary in the continental realm of the southern Karoo Basin, South Africa. Paleoworld 16, 67–104.

De Kock, M.O., Kirschvink, J.L., 2004. Paleomagnetic constraints on the Permian-Triassic boundary in terrestrial strata of the Karoo Supergroup, South Africa: implications for causes of the end-Permian extinction event. Gondwana Res. 7, 175–183.

Draper, J.J., Jensen, A.R., 1994. The geochemistry of Lake Frome, a playa lake in South Australia. BMR J. Aust. Geol. Geophys. 1, 83–104.

Dunlop, D.J., 1971. Magnetic properties of fine particle hematite. Ann. Geophys. 27, 269–293.

Gastaldo, R.A., Neveling, J., 2012. The terrestrial Permian-Triassic boundary event is a nonevent: reply. Geology 40, e257. http://dx.doi.org/10.1130/G32975Y.1.

Gastaldo, R.A., Neveling, J., 2016. Comment on “anatomy of a mass extinction: sedimentological and taphonomic evidence for drought-induced die-offs at the Permo-Triassic boundary in the main Karoo Basin, South Africa” by R.M.H. Smith and J. Botha-Brink. Palaeogeogr. Palaeoclimatol. Palaeoecol. 396, 99–118.

Gastaldo, R.A., Rolerson, M.W., 2008. *Katbergia* gen. Novol., a new trace fossil from upper Permian and lower Triassic rocks of the Karoo Basin: implications for palaeoenvironmental conditions at the P/Tr extinction event. Palaeontology 51, 215–229.

Gastaldo, R.A., Adendorff, R., Bamford, M.K., Labandeira, C.C., Neveling, J., Sims, H.J., 2005. Taphonomic trends of macrofloral assemblages across the Permian-Triassic boundary, Karoo Basin, South Africa. PALAIOS 20, 478–497. http://dx.doi.org/10.1016/j.palaeo.2010.03.052.

Gastaldo, R.A., Neveling, J., Clark, K., Newbury, S.S., 2009. The terrestrial Permian-Triassic boundary event bed is a nonevent. Geology 37 (3), 199–202.

Gastaldo, R.A., Knight, C.L., Neveling, J., Tabor, N.J., 2014. Latest Permian paleosols from Wapadsberg Pass, South Africa: implications for changhsingian climate. Geol. Soc. Am. Bull. 126 (5/6), 665–679.

Gastaldo, R.A., Kamo, S.L., Neveling, J., Geissman, J.W., Bamford, M., Looy, C.V.O.L., 2015. Is the vertebrate-defined Permian-Triassic boundary in the Karoo Basin, South Africa, the terrestrial expression of the end-Permian marine event? Geology 43, 939–942. http://dx.doi.org/10.1130/G37040.1.

Gastaldo, R.A., Neveling, J., Looy, C.V.O.L., Bamford, M.K., Kamo, S.L., Geissman, J.W., 2017. Paleontology of the Blaauwater 67 Farm, South Africa: testing the daptocephalus/lystrosaurus biozone boundary in a stratigraphic framework. PALAIOS 34, 349–366.

Gaupp, R., Gast, R., Forster, C., 2000. Late Permian playa lake deposits of the southern Permian Basin (Central Europe). AAPG Stud. Geol. 46, 75–86.

Gill, T.E., Gillette, D.A., Niemeyer, T., Winn, R.T., 2002. Elemental geochemistry of wind-erodible playa sediments, Owens Lake, California. Nucl. Instrum. Methods Phys. Res., Sect. B 189, 209–213.

Gresse, P.G., Theron, J.N., Fitch, F.J., Miller, J.A., 1992. Tectonic inversion and

radiometric resetting of the basement in the Cape Fold Belt. In: de Wit, M.J., Ransome, I.G.D. (Eds.), Inversion Tectonics of the Cape Fold Belt, Karoo and Cretaceous Basins of Southern Africa. A.A. Balkema, Rotterdam, pp. 217–228.
Hälbich, I.W., 1983. A tectogenesis of the Cape Fold Belt. In: Söhnge, A.P.G., Hälbich, I.W. (Eds.), Geodynamics of the Cape Fold Belt. 12. Geological Society of South Africa, Special Publication, pp. 165–175.
Hiete, M., Berner, U., Heunisch, C., Roehling, H.G., 2006. A high-resolution inorganic geochemical profile across the Zechstein-Buntsandstein boundary in the North German Basin. Z. Dtsch. Ges. Geowiss. 157, 44–105.
Hiller, N., Stavrakis, N., 1984. Permo-Triassic fluvial systems in the southeastern Karoo Basin, South Africa. Palaeogeogr. Palaeoclimatol. Palaeoecol. 45, 1–21.
Hotton, N., 1967. Stratigraphy and sedimentation in the Beaufort series (Permian-Triassic), South Africa. In: Teichert, C. (Ed.), Essays in Paleontology and Stratigraphy. 2. University of Kansas Department of Geology Special Publication, pp. 390–428 IGC.
Hounslow, M.W., Balabanov, Y.P., 2016. A geomagnetic polarity timescale for the Permian, calibrated to stage boundaries. In: Lucas, S.G., Shen, S.Z. (Eds.), The Permian Timescale. 450 Geological Society, London, Special Publication. 8 December 2016. http://dx.doi.org/10.1144/SP450.8.
Johnson, M.R., van Vuuren, C.J., Visser, J.N.J., Cole, D.I., de Wickens, H.V.O.L., Christie, A.D.M., Roberts, D.L., Brandl, G., 2006. Sedimentary rocks of the Karoo Supergroup. In: Johnson, M.R., Anhaeusser, C.R., Thomas, R.J. (Eds.), The Geology of South Africa: the Geological Society of South Africa, Johannesburg, and the Council for Geoscience, Pretoria, pp. 461–499.
Kammerer, C.F., Angielczyk, K.D., Fröbisch, J., 2011. A comprehensive taxonomic revision of *Dicynodon* (Therapsida, Anomodontia) and its implications for dicynodont phylogeny, biogeography, and biostratigraphy. J. Vertebr. Paleontol. 31, 1–158.
Keyser, A.W., 1981. The stratigraphic distribution of the Dicynodontia of Africa reviewed in a Gondwana context. In: Creswell, M.M., Vella, P. (Eds.), Gondwana Five. A.A. Balkema, Rotterdam, pp. 61–64.
Keyser, A.W., Smith, R.H.M., 1978. Vertebrate biozonation of the beaufort group with special reference to the Western Karoo Basin. Ann. Geol. Survol. 12 (1977–1978), 1–35.
Kistler, R.B., Helvaci, C., 1994. Boron and Borates. In: Carr, D.D. (Ed.), Industrial Minerals and Rocks: Society of Mining, Metallurgy, and Exporation, 6th ed. pp. 171–186.
Kitching, J.W., 1971. A short review of the Beaufort zoning in South Africa. In: Haughton, S.H. (Ed.), Second Gondwana Symposium, Proceedings & Papers, pp. 309–312.
Kitching, J.W., 1977. The distribution of the Karoo vertebrate fauna: Memoir of the Bernard Price Institute for Palaeontological Research. 1. University of the Witwatersrandpp. 1–131.
Konrád, G., Sebe, K., Halász, A., Babinszki, E., 2010. Sedimentology of a Permian playa lake: the Boda claystone formation, Hungary. Geologos 16, 27–41.
Kraus, M.J., Hasiotis, S.T., 2006. Significance of different modes of rhizolith preservation to interpreting paleoenvironmental and paleohydrological settings: examples from Paleogene paleosols, Bighorn Basin, Wyoming, USA. J. Sediment. Res. 76, 633–646.
Kutty, T.S., 1972. Permian reptilian fauna from India. Nature 237, 462–463.
Li, J., Gastaldo, R.A., Neveling, J., Geissman, J.W., 2017. Green or red: the change in siltstone color across the *Daptocephalus* (*Dicynodon*) and *Lystrosaurus* assemblage zones, Karoo Basin, South Africa, is not a function of aridification. J. Sediment. Res. 87, 653–671.
Lisle, R.J., Brabham, P.J., Barnes, J.W., 2011. Basic Geological Mapping, fifth edition. John Wiley & Sons, Ltd., New York (217 p.).
Lopez, M., Gand, G., Garric, J., Körner, F., Schneider, J., 2008. The playa environments of the Lodève Permian basin (Languedoc-France). J. Iber. Geol. 34, 29–56.
Lucas, S.G., 1997. *Dicynodon* and late Permian Pangea. In: Wang, N., Remane, J. (Eds.), Stratigraphy: Proceedings of the 30th International Geological Congress. vol. 11. pp. 133–141.
Lucas, S.G., 2006. Global Permian tetrapod biostratigraphy and biochronology. In: Lucas, S.G., Cassinis, G., Schneider, J.W. (Eds.), Non-marine Permian Biostratigraphy and Biochronology. vol. 265. Geological Society of London, Special Publication, pp. 65–93.
Lucas, S.G., 2017a. Permian tetrapod extinction events. Earth Sci. Revol. 170, 31–60.
Lucas, S.G., 2017b. Permian tetrapod biochronology, correlation and evolutionary events. In: Lucas, S.G., Shen, S.Z. (Eds.), The Permian Timescale. 450 Geological Society, London, Special Publications (doi.org/10.1144/SP450.12).
Mack, G.H., James, W.C., Monger, H.C., 1993. Classification of paleosols. Geol. Soc. Am. Bull. 105, 129–136.
Nesbitt, W., Young, G.M., 1982. Early Proterozoic climates and plate motions inferred from major element chemistry of lutites. Nature 299, 715–717.
Neveling, J., Gastaldo, R.A., Geissman, J.W., 2016a. Permo–Triassic boundary in the Karoo Basin. In: Field Trip Guide Pre-3. Council for Geoscience, Pretoria, South Africa (81 p.). 10.13140/RG.2.2.22414.15683.
Neveling, J., Gastaldo, R.A., Kamo, S.L., Geissman, J.W., Looy, C.V.O.L., Bamford, M.K., 2016b. A review of stratigraphic, geochemical, and paleontologic correlations data of the terrestrial end-permian record in the Karoo Basin, South Africa. In: de Wit, M., Linol, B. (Eds.), The Origin and Evolution of the Cape Mountains and Karoo Basin. Springer Publishing, pp. 151–157.
Newell, A.J., Sennikov, A.G., Benton, M.J., Molostovskaya, I.I., Golubev, V.O.L.K., Minikh, A.V.O.L., Minikh, M.G., 2010. Disruption of playa–lacustrine depositional systems at the Permo-Triassic boundary: evidence from Vyazniki and Gorokhovets on the Russian Platform. J. Geol. Soc. Lond. 167, 695–716.
Ozdemir, O., Dunlop, D.J., 2014. Hysteresis and coercivity of hematite. J. Geophys. Res. 119, 2582–2594. http://dx.doi.org/10.1002/2013JB010739.
Pace, D.W., Gastaldo, R.A., Neveling, J., 2009. Early Triassic aggradational and degradational landscapes of the Karoo basin and evidence for climate oscillation following the P-Tr event. J. Sediment. Res. 79, 316–331.
Pollastro, R.M., 1982. A recommended procedure for the preparation of oriented clay-mineral specimens for X-ray diffraction analysis: modifications to Drever's filter-membrane peel technique. In: Open-File Report. United States Department of the Interior Geological Survey (82–71).
Reinhardt, L., Ricken, W., 2000. The stratigraphic and geochemical record of playa cycles: monitoring a Pangaean monsoon-like system (Triassic, Middle Keuper, S. Germany). Palaeogeogr. Palaeoclimatol. Palaeoecol. 161, 205–227.
Retallack, G.J., Smith, R.M.H., Ward, P.D., 2003. Vertebrate extinction across Permian-Triassic boundary in Karoo Basin, South Africa. Geol. Soc. Am. Bull. 115, 1133–1152.
Rey, K., Amiot, R., Fourel, F., Rigaudier, T., Abdala, F., Day, M.O., Fernandez, V.O.L., Fluteau, F., France-lanord, C., Rubidge, B.S., Smith, R.M., Viglietti, P.A., Zipfel, B., Lécuyer, C., 2016. Global climate perturbations during the Permo-Triassic mass extinctions recorded by continental tetrapods from South Africa. Gondwana Res. 37, 384–396. (GR-01523.). http://dx.doi.org/10.1016/j.gr.2015.09.008.
Roopnarine, P.D., Angielczyk, K.D., 2015. Community stability and selective extinction during the Permian-Triassic mass extinction. Science 350, 90–93. http://dx.doi.org/10.1126/science.aab1371.
Rubidge, B.S., 1995, Biostratigraphy of the Beaufort group (Karoo supergroup): South African Committee for Stratigraphy, Biostratigraphic Ser., n. 1, (46 p.).
Rubidge, B.S., Erwin, D.H., Ramezani, J., Bowring, S.A., de Klerk, W.J., 2013. High-precision temporal calibration of late Permian vertebrate biostratigraphy: U-Pb zircon constraints from the Karoo Supergroup, South Africa. Geology 41, 363–366.
Rubidge, B.S., Day, M.O., Barbolini, N., Hancox, P.J., Choiniere, J., Bamford, M.K., Viglietti, P.A., McPhee, B., Jirah, S., 2016. Advances in nonmarine Karoo biostratigraphy: significance for Understanding Basin development. In: de Wit, M., Linol, B. (Eds.), The Origin and Evolution of the Cape Mountains and Karoo Basin. Springer Publishing, pp. 141–150 (Chapter 19).
Schneider, J.W., Körner, F., Roscher, M., Kroner, U., 2006. Permian climate development in the northeastern peri-Tethys area — the Lodève basin, French Massif Central, compared in a European and global context. Palaeogeogr. Palaeoclimatol. Palaeoecol. 240, 161–183.
Schwindt, D.M., Rampino, M.R., Steiner, M.B., Eshet, Y., 2003. Stratigraphy, paleomagnetic results, and preliminary palynology across the Permian–Triassic (P–Tr) boundary at Carlton Heights, southern Karoo Basin (South Africa). In: Koeberl, C., Martínez-Ruiz, F.C. (Eds.), Impact Markers in the Stratigraphic Record, Impact Studies 2003. Springer Verlag, pp. 293–314.
Sheldon, N.D., Tabor, N.J., 2009. Quantitative paleoenvironmental and paleoclimatic reconstruction using paleosols. Earth Sci. Revol. 95, 1–52.
Shen, S.Z., Crowley, J.L., Wang, Y., Bowring, S.A., Erwin, D.H., Sadler, P.M., Cao, C.Q., Rothman, D.H., Henderson, C.M., Ramezani, J., Zhang, H., Shen, Y., Wang, X.D., Wang, W., Mu, L., Li, W.Z., Tang, Y.G., Liu, X.L., Liu, L.J., Zeng, Y., Jiang, Y.F., Jin, Y.G., 2011. Calibrating the end-Permian mass extinction. Science 334, 1367–1372.
Shütt, B., 2004. The chemistry of playa-lake sediments as a tool for the reconstruction of Holocene environmental conditions – a case study from the central Ebro basin. In: Smykatz-Kloss, W., Felix-Henningsen, P. (Eds.), Paleoecology of Quaternary drylands: Lecture Notes in Earth Sciences. vol. 102. pp. 5–30.
Smith, R.M.H., 1987. Morphology and depositional history of exhumed Permian point bars in the southwestern Karoo, South Africa. J. Sediment. Petrol. 57, 19–29.
Smith, R.M.H., 1995. Changing fluvial environments across the Permian-Triassic boundary in the Karoo Basin, South Africa and possible causes of tetrapod extinctions. Palaeogeogr. Palaeoclimatol. Palaeoecol. 117, 81–104.
Smith, R.M.H., Botha, J., 2005. The recovery of terrestrial vertebrate diversity in the South African Karoo Basin after the end-Permian extinction. C.R. Palevol 4, 555–568.
Smith, R.M.H., Botha-Brink, J., 2014. Anatomy of a mass extinction: sedimentological and taphonomic evidence for drought-induced die-offs at the Permo-Triassic boundary in the main Karoo Basin, South Africa. Palaeogeogr. Palaeoclimatol. Palaeoecol. 396, 99–118.
Smith, R.M.H., Keyser, A.W., 1995. Biostratigraphy of the Cistecephalus Zone. In: Rubidge, B.S. (Ed.), Biostratigraphy of the Beaufort Group (Karoo Supergroup). 1. South African Committee for Stratigraphy, pp. 213–228.
Smith, R.M.H., Ward, P.D., 2001. Pattern of vertebrate extinctions across an event bed at the Permian-Triassic boundary in the Karoo Basin of South Africa. Geology 29 (12), 1147–1150.
Smykatz-Kloss, W., Roy, P.D., 2010. Evaporite mineralogy and major element geochemistry as tools for palaeoclimatic investigations in arid regions: a synthesis. Bol. Soc. Geol. Mex. 62, 379–390.
Steiner, M.B., Eshet, Y.U., Rampino, M.R., Schwindt, D.M., 2003. Fungal abundance spike and the Permian–Triassic boundary in the Karoo Supergroup (South Africa). Palaeogeogr. Palaeoclimatol. Palaeoecol. 194, 405–414.
Szurlies, M., 2013, Late Permian (Zechstein) Magnetostratigraphy in Western and Central Europe: Geological Society of London Special Publication, vol. 376, or doi:http://dx.doi.org/10.1144/SP376.7.
Tabor, N.J., Montañez, I.P., Steiner, M., Schwindt, D., 2007. The $d^{13}C$ values of Permo-Triassic carbonates from South Africa reflect a stinking, sulfurous swamp, not atmospheric conditions. Palaeogeogr. Palaeoclimatol. Palaeoecol. 225, 370–381.
Tucker, M.E., 2011. Sedimentary Rocks in the Field: A Practical Guide: The Geological Field Guide Series. Wiley-Blackwell, Oxford, UK (276 p.).
Turner, B.R., Smith, D.B., 1997. A playa deposit of pre-Yellow Sands age (upper Rotliegend/Weissliegend) in the Permian of northeast England. Sediment. Geol. 114, 305–319.
Varga, A.R., Raucsik, B., Máthé, Z., 2005. Chemical composition, provenance and early diagnetic processes of playa lake deposits from the Boda Siltstone Formation (Upper Permian), SW Hungary. Acta Geol. Hung. 48/1, 49–68.
Viglietti, P.A., Smith, R.M.H., Angielczyk, K.D., Kammerer, C.F., Fröbisch, J., Rubidge, B.S., 2016. The *Daptocephalus* assemblage zone (Lopingian), South Africa: A proposed biostratigraphy based on a new compilation of stratigraphic ranges. J. Afr. Earth Sci. 113, 153–164.

Ward, P.D., Montgomery, D.R., Smith, R.M.H., 2000. Altered river morphology in South Africa related to the Permian-Triassic extinction. Science 289, 1740–1743.
Ward, P.D., Botha, J., Buick, R., De Kock, M.O., Erwin, D.H., Garrison, G.H., Kirschvink, J.L., Smith, R.M.H., 2005. Abrupt and gradual extinction among late Permian land vertebrates in the Karoo Basin, South Africa. Science 307, 709–714.
Ward, P.D., Retallack, G.J., Smith, R.M.H., 2012. The terrestrial Permian–Triassic boundary event bed is a nonevent: COMMENT. Geology 40, e256.
Zhang, G., Buatois, L.A., Mángano, M.G., Aceñola, F.G., 1998. Sedimentary facies and environmental ichnology of a? Permian playa-lake complex in western Argentina. Palaeogeogr. Palaeoclimatol. Palaeoecol. 138, 221–243.